

Dynamics of inertial active particles in a microchannel with Poiseuille flow

by

Harshita Tiwari and Sanket Biswas
(GCT/1940097 and GCT/1940108)

under the supervision of

Dr. Kamlesh Kumari



Department of Chemical Engineering
Sant Longowal Institute of Engineering and Technology (SLIET)

Longowal, Sangrur, Punjab

May 2023

Dynamics of inertial active particles in a microchannel with Poiseuille flow

by

Harshita Tiwari¹ and Sanket Biswas²
(GCT/1940097 and GCT/1940108)



under the supervision of

Dr. Kamlesh Kumari³
Professor

Department of Chemical Engineering
Sant Longowal Institute of Engineering and Technology (SLIET)

A project report submitted to the
Department of Chemical Engineering
Sant Longowal Institute of Engineering and Technology (SLIET), Longowal
in fulfillment of the
BE Project Stage II (PRCH-721) requirement for the degree of
Bachelor of Engineering (BE) in Chemical Engineering

Longowal, Sangrur, Punjab
May 2023

¹Email address: 1940097@sliet.ac.in

²Email address: 1940108@sliet.ac.in

³Email address: kamlesh213@sliet.ac.in

Abstract

This thesis investigates the swimming dynamics of inertial active Brownian particles (ABPs) in a microchannel subjected to a pressure-driven Poiseuille flow. The study aims to understand the behavior of these particles in realistic environments and contributes to the fields of active matter and inertial microfluidics. The research begins with a background and motivation section, highlighting the research gap and the importance of studying inertial ABPs in this context. The theoretical framework extends the active Langevin model to include inertial effects and incorporates Gaussian white noise and sliding-reflecting boundary conditions. Finite-difference equations are developed for numerical simulations. The simulation results focus on four ABPs, including one non-inertial and three inertial particles with increasing masses. Various flow conditions, temperatures, and initial conditions are considered. Trajectories, phase portraits, and statistical analyses provide insights into the stochastic dynamics of the particles. The study fills a crucial gap in understanding the behavior of inertial ABPs in a microchannel with Poiseuille flow and contributes to the development of accurate models. The findings have implications for designing microfluidic devices and systems in fields such as targeted drug delivery, biomedical diagnostics, environmental monitoring, energy conversion, and food processing.

Examining Committee Membership

The following served on the Examining Committee for this report. The decision of the Examining Committee is by majority vote.

Internal Examiners:	Dr. Pushpa Jha Professor and HoD, Dept. of Chemical Engineering, SLIET Longowal Dr. Sandeep Mohan Ahuja Professor, Department of Chemical Engineering, SLIET Longowal
Project Supervisor:	Dr. Kamlesh Kumari Professor, Department of Chemical Engineering, SLIET Longowal

Authors' Declaration

We declare that the contents of this report are original and have been produced solely by us. We further attest that, to the best of our knowledge and belief, it does not contain any previously published material or work written by another person, nor does it consist of material that has been accepted for the award of any other degree or diploma from this university or any other institute of higher learning, unless we have appropriately acknowledged and referenced such material in the text.

Harshita Tiwari

Ms. Harshita Tiwari
(GCT/1940097)

.....
14/05/2023

Date

Sanket Biswas

Mr. Sanket Biswas
(GCT/1940108)

.....
14/05/2023

Date

Acknowledgements

We would like to express our gratitude to all those who have supported and guided us throughout this project. First and foremost, we extend our deepest thanks to our esteemed project supervisor Dr. Kamlesh Kumari for granting us the opportunity to work on a fascinating project in active matter and microfluidics. Her diligent guidance on numerous scientific questions served as hooks in our research, and we are grateful for her prompt responses to our queries and questions. We commend her patience and encouragement as she challenged us to think critically and provided regular constructive feedback on our weekly project reports. Her feedback has been a catalyst for our personal and professional growth, and we feel honored to have had her as our supervisor.

We also acknowledge and extend our sincere appreciation to Prof. Shubhadeep Mandal and Prof. Aloke Kumar for their invaluable support and dedication throughout our project. Their expertise and guidance have been instrumental in shaping our understanding of our research work and its potential applications in various fields. We are extremely grateful for their invaluable support and unconventional thinking, which enabled us to establish a strong rapport with them based on open and trusting communication.

We also express our gratitude to the graduate students and project assistants of Complex & Biological Fluids Lab (Prof. Shubhadeep Mandal's Lab) and Prof. Aloke Kumar's Lab at IISc for their immense support and friendship during the completion of this work. Their selfless mentorship and guidance have been instrumental in our research progress, and we are indebted to them.

Finally, we would like to acknowledge and thank our family and friends for their constant and unwavering encouragement throughout our journey as aspiring researchers. Their unwavering support has been a constant source of inspiration and motivation, and we owe them a debt of gratitude for their role in our success. We will always cherish their support and encouragement.

Certificate

This is to certify that, Ms. Harshita Tiwari (GCT/1940097) and Mr. Sanket Biswas (GCT/1940108), both of whom are pursuing a Bachelor of Engineering (BE) in Chemical Engineering from Sant Longowal Institute of Engineering and Technology (SLIET) have successfully completed their BE Project Stage II (Jan. '23 to Jun. '23) on the *Dynamics of inertial active particles in a microchannel with Poiseuille flow* at the Department of Chemical Engineering, Sant Longowal Institute of Engineering and Technology (SLIET), Longowal. They have successfully presented their work at the BE Project Seminar and have also submitted a hard copy and a soft copy of this report for further reference and record. The final evaluation was done offline at the Department of Chemical Engineering of SLIET by a select and experienced group of faculties of the department.

.....
Dr. Kamlesh Kumari
(Project Supervisor)

.....
Date

Table of Contents

1	Introduction	1
1.1	Background and motivation	1
1.2	Overview of our research	4
1.3	Mapping of COs and POs	4
2	Mathematical and numerical simulation framework	5
2.1	Mathematical framework	5
2.1.1	Geometrical setup	5
2.1.2	Equations of motion	6
2.1.3	Non-dimensionalisation	7
2.2	Numerical simulation framework	8
2.2.1	Finite difference equations	8
2.2.2	Reflective boundaries	9
2.3	Inertialess equations of motion	11
2.3.1	Non-dimensionalisation	12
2.3.2	Finite difference equations	12
3	Results and discussions	13
3.1	Trajectories and phase spaces	13
3.2	Statistical analysis	23

3.2.1	Mean squared displacement (MSD)	23
3.2.2	Velocity autocorrelation function (VACF)	27
3.2.3	Joint probability distribution function (JPDF) of the phase space	30
4	Appendix	39
References		40

Chapter 1

Introduction

This research paper seeks to investigate the swimming dynamics of *inertial active Brownian particles* in a microchannel subjected to a pressure-driven Poiseuille flow. In contrast to *non-inertial active Brownian particles*, which are unaffected by their mass and moment of inertia in a microchannel with Poiseuille flow, *inertial active Brownian particles* have sufficient mass and moment of inertia that can significantly alter their swimming trajectories. This chapter is divided into three main sections, namely, background and motivation, overview of our research, and mapping of COs and POs, that aim to introduce and contextualize our study.

1.1 Background and motivation

This section discusses the rationale behind our research work, highlighting the research gap in the existing literature and the importance of understanding the dynamics of inertial active Brownian particles in a microchannel with Poiseuille flow. Our research questions and objectives are presented, aiming to contribute to the advancement of knowledge in the fields of *active matter* and *inertial microfluidics*.

In the past few decades, the study of active particles in the low Reynolds number regime has gained significant attention from various fields, including applied mathematics, biology, physics, mechanical engineering, and chemical engineering [1–6]. These particles are capable of converting energy from their surroundings into directed motion, allowing them to swim independently without external forces [7–13]. In this regime, their dynamics are dominated by the viscous force of the surrounding fluid medium rather than the inertia from the particle's mass [14].

Active particles experience dynamic fluid environments and confinements, requiring them to use various propulsion mechanisms to move through them. Examples of these mechanisms include ciliated microorganisms that use metachronal waves generated by the synchronous beating of cilia to move through laminar flow in a porous matrix [15–17], sperm cells that use flagella to swim through the fallopian tubes [12, 18], and bacteria that use a run-and-tumble mechanism to move through lung mucus [19, 20]. Researchers have also developed artificial self-propelled micro- and nanoparticles to better understand and mimic the dynamics of these particles, including their collective behavior, such as biofilm formation or intriguing collective patterns, and their interactions with micro-scale flows and boundaries [21, 22]. In addition, artificial self-propelled particles have been utilized in various technological domains, including but not limited to targeted drug delivery [23, 24], environmental remediation [25–27], microfluidic systems [28–31], biomedical equipments [32, 33], microrobotics [34, 35], energy harvesting [36, 37], and oil spill cleanup [38–40].

At low Reynolds number, the dynamics of active particles is overdamped and is significantly different from those of (overdamped) passive particles, such as gas molecules [41–43], passive colloids [44, 45], pollen grains [46], proteins [47, 48], DNA molecules [49, 50], and other biomolecules. Passive particles move solely due to thermal fluctuations in the surrounding fluid and do not actively propel themselves, displaying pure diffusive behaviour. They exhibit Brownian motion, which is characterized by random movements due to collisions with the surrounding fluid molecules. In contrast, active particles typically exhibit persistent single-particle trajectories [4, 51, 52]. Specifically, active particles tend to move persistently in one spatial direction with a velocity known as the *self-propelled velocity* and only randomize their direction of motion after a certain time, referred to as the *persistence time*. These features have been identified as the fundamental components needed to construct coarse-grained models within the framework of stochastic processes, which can capture the essential behavior of this class of active systems. Among them, the *active Brownian particle (ABP) model* [53–61] is one of the most popular descriptions used to capture the essential behavior of this class of active systems. The ABP model introduces the *activity* as a time-dependent force of constant magnitude with a stochastic evolution of its direction. Its popularity is attributed to its simplicity, while also providing an accurate representation of active colloids [62–66] and bacteria [4] subject to both translational and rotational Brownian motion.

It is noteworthy that active motion is not confined to microscopic scales, as it is also observable at mesoscopic and macroscopic scales. Examples of mesoscopic active motion include the collective behavior of cells, such as the alignment of fibroblasts and the migration of epithelial cells [67]. Additionally, mesoscopic systems such as microtubules and kinesin motor proteins also exhibit active motion [68, 69]. On the macroscopic scale, examples of

active motion include flocking birds, schooling fish, and swarming insects, which exhibit collective behavior through the interaction of individuals [70]. At these scales, motion is no longer at a low Reynolds number, and inertial effects become dominant in the dynamics, necessitating their inclusion in the modelling. These particles are referred to as *microflyers*, *hoppers*, or *runners* [71], and their dynamics are underdamped, but their motion is still affected by random fluctuations in the surrounding medium. To capture their dynamics, the influence of the particle's mass on translational motion [72–79] and moment of inertia on rotational velocity [80–86] has been considered in the ABP model. This extension of the ABP model is referred to as the *active Langevin model* or the *inertial ABP model* [71, 87].

In recent years, there has been an increasing interest in the theoretical description of inertial effects in the dynamics of mesoscopic and macroscopic systems, as well as a growing number of experimental observations highlighting the importance of inertia in these systems [71, 88–90]. The study of inertial active particles in various physical confinements is critical to understanding the effect of boundaries on their dynamics and for applications to real-life systems [91–96]. Confinements in microfluidic devices, including microchannels with Poiseuille flow, are a common feature, making it important to understand the behavior of inertial active particles in these environments. The presence of Poiseuille flow has been shown to significantly affect the dynamics of non-inertial active particles in microchannels [97, 98]. However, there is a lack of concrete theoretical descriptions of the dynamics of inertial active particles in microchannels with Poiseuille flow.

Inertial active particles have numerous potential applications in microfluidic devices and systems, including targeted drug delivery, biomedical diagnostics, environmental monitoring, energy conversion, and food and beverage processing. For example, inertial active particles can be used as a platform for targeted drug delivery in cancer treatment, where drug-loaded microcapsules can be directed to specific cancer cells using external magnetic fields, ultrasound, or other methods. They can also be used in microfluidic devices for diagnosing diseases or infections, monitoring water quality or air pollution, and harvesting energy from flowing fluids. In addition, inertial active particles can be used in microfluidic systems for processing and filtering food and beverage products to improve their quality and safety.

Therefore, in this study, we investigate the behavior of inertial active particles in microchannels with Poiseuille flow to fill the gap in theoretical descriptions of the dynamics of these particles and gain insights into their behavior in realistic environments. The insights gained from this study can aid in the development of more accurate models for predicting the behavior of inertial active particles and designing effective microfluidic devices and systems.

1.2 Overview of our research

In this research, we investigate the dynamics of inertial active Brownian particles (ABPs) in microchannels with Poiseuille flow. Our work builds upon the mathematical framework presented in [97] and extends the inertial ABP model proposed in [87] to incorporate the effect of Poiseuille flow in microchannels on their dynamics.

Chapter 2 outlines the non-dimensionalized equations of motion (EOMs) required to study the dynamics of inertial ABPs in microchannels with Poiseuille flow. These EOMs include Gaussian white noises to account for the stochasticity in their Brownian motion, and sliding-reflecting boundary conditions to model their collisional dynamics with the microchannel walls [97, 99–101]. To simulate the dynamics of the inertial ABPs, we develop finite-difference equations (FDEs) based on the numerical simulation framework presented in [99, 102]. These FDEs can be implemented using MATLAB, COMSOL Multiphysics, or any other suitable simulation software.

Finally, in Chapter 3, we present the results obtained from simulations (in MATLAB) of four active Brownian particles, including one non-inertial particle and three inertial particles with increasing masses (1.5×10^{-10} kg, 1.5×10^{-9} kg, and 1.5×10^{-8} kg), under various flow conditions, temperatures, and initial conditions. We examine the trajectories and phase portraits of the particles and analyze their stochastic dynamics using statistical tools such as mean squared displacement (MSD), velocity autocorrelation function (VACF), and joint probability distribution function (JPDF).

1.3 Mapping of COs and POs

After conducting a comprehensive analysis of the research background, motivation, problem statements, achieved objectives, scope and potential applications of our study, as well as possibilities for future research, we have concluded that our work is consistent with the predefined program objectives (POs) and course objectives (COs), which are detailed below:

POs & COs	PO1	PO2	PO3	PO4	PO5	PO6	PO7	PO8	PO9	PO10	PO11	PO12	PSO1	PSO2
CO1	S	S	W	S	S	M	S	S	S	S	M	M	M	S
CO2	S	S	S	S	S	S	S	M	S	S	M	M	M	S
CO3	S	M	M	S	S	M	S	S	S	S	M	M	M	S

Chapter 2

Mathematical and numerical simulation framework

2.1 Mathematical framework

2.1.1 Geometrical setup

We consider a spherical inertial self-propelled particle of radius R in two spatial dimensions, say x - y plane, in a rectangular microchannel with pressure-driven Poiseuille flow, given by

$$\mathbf{v}_f = v_f \left(1 - \frac{4y^2}{L^2}\right) \hat{\mathbf{e}}_x, \quad (2.1)$$

where L is the height of the channel and $v_f = |\mathbf{v}_f(0)|$ is the centre-line flow speed. The flow velocity vanishes at the channel walls, located at $y = \pm L/2$, due to the no-slip boundary conditions. Further, the corresponding vorticity is given by

$$\omega_s = \frac{4v_f y}{L^2}. \quad (2.2)$$

The particle under consideration is characterised by its mass m and moment of inertia J . Let $\mathbf{r} = (x, y)$ denote the centre-of-mass position, θ the orientational angle (with respect to the positive x axis), $\mathbf{n} = (\cos \theta, \sin \theta)$ the orientation vector, v_0 the self-propelled speed, and Ω the active rotational velocity of the particle. Therefore, the self-propelled velocity of the particle is given by $\mathbf{v}_0 = v_0 \mathbf{n}$. For non-chiral particles, $\Omega = 0$, and for chiral particles, $\Omega \neq 0$.

The position $\mathbf{r}(t)$ of the particle undergoes Brownian diffusion with translational diffusion coefficient

$$D_T = \frac{k_B T}{\gamma} \text{ (Einstein relation),} \quad (2.3)$$

where k_B is the Boltzmann constant, T is the temperature, and $\gamma = 6\pi\mu R$ is the translational friction coefficient with μ being the fluid viscosity. Moreover, the orientation $\theta(t)$ of the particle undergoes rotational diffusion with rotational diffusion coefficient

$$D_R = \frac{k_B T}{\gamma_R}, \quad (2.4)$$

where $\gamma_R = 8\pi\mu R^3$ is the rotational friction coefficient.

2.1.2 Equations of motion

Neglecting all external forces in the inertial ABP model, the translational motion of the particle is given by

$$\dot{\mathbf{r}} = \mathbf{v}, \quad (2.5a)$$

$$m\dot{\mathbf{v}} = \gamma(\mathbf{v}_f - \mathbf{v}) + \gamma\sqrt{2D_T}\boldsymbol{\xi} + \gamma v_0 \mathbf{n}, \quad (2.5b)$$

where $\gamma(\mathbf{v}_f - \mathbf{v})$ is the friction force, $\gamma\sqrt{2D_T}\boldsymbol{\xi}$ is the thermal force, and $\gamma v_0 \mathbf{n}$ is the active force. Similarly, the rotational motion is given by

$$\dot{\theta} = \omega, \quad (2.6a)$$

$$J\dot{\omega} = \gamma_r(\omega_s - \omega) + \gamma_r\sqrt{2D_R}\boldsymbol{\eta} + \gamma_r\Omega, \quad (2.6b)$$

where $\gamma_r(\omega_s - \omega)$ is the friction torque, $\gamma_r\sqrt{2D_R}\boldsymbol{\eta}$ is the stochastic torque, and $\gamma_r\Omega$ is the active torque yielding the deterministic circular motion of the particle. Here, $\boldsymbol{\xi}$ and $\boldsymbol{\eta}$ represent independent Gaussian white noises with zero mean and unit variance.

At this point, we introduce three typical times by which the inertial ABP model is characterized:

$$\tau_P = \frac{1}{D_R}, \quad \tau_R = \frac{J}{\gamma_r}, \quad \tau = \frac{m}{\gamma}, \quad (2.7)$$

where τ_p is known as the *persistence time*, τ_R is known as the *orientational relaxation time*, and τ is known as the *translational relaxation time*.

So, component-wise, we have the following governing equations of motion:

$$\frac{dx}{dt} = v_x, \quad \frac{dy}{dt} = v_y, \quad \frac{d\theta}{dt} = \omega, \quad (2.8a)$$

$$\tau \frac{dv_x}{dt} = -v_x + v_f \left(1 - \frac{4y^2}{L^2} \right) + \sqrt{2D_T} \xi_x + v_0 \cos \theta, \quad (2.8b)$$

$$\tau \frac{dv_y}{dt} = -v_y + \sqrt{2D_T} \xi_y + v_0 \sin \theta, \quad (2.8c)$$

$$\tau_R \frac{d\omega}{dt} = -\omega + \frac{4v_f y}{L^2} + \sqrt{2D_R} \eta + \Omega, \quad (2.8d)$$

where $\mathbf{v} = (v_x, v_y)$ and $\boldsymbol{\xi} = (\xi_x, \xi_y)$.

2.1.3 Non-dimensionalisation

We consider a dimensionless description of the governing equations of motion, i.e. Eqn. (2.8), by rescaling all the relevant variables as follows:

$$X = \frac{x}{L}, \quad Y = \frac{y}{L}, \quad T = \frac{v_0 t}{L}, \quad V_x = \frac{v_x}{v_0}, \quad V_y = \frac{v_y}{v_0}, \quad \text{and } \chi = \frac{L\omega}{v_0}.$$

The other rescaled parameters are as follows:

$$D_t = \frac{D_T}{Lv_0}, \quad D_r = \frac{LD_R}{v_0}, \quad V_f = \frac{v_f}{v_0}, \quad \text{and } \mathcal{M} = \frac{L\Omega}{v_0}.$$

Using these dimensionless variables and parameters, the equations of motion can be rewritten as follows:

$$\frac{dX}{dT} = V_x, \quad \frac{dY}{dT} = V_y, \quad \frac{d\theta}{dT} = \chi, \quad (2.9a)$$

$$\frac{dV_x}{dT} = -\alpha \left[V_x - V_f(1 - 4Y^2) - \sqrt{2\kappa D_t} \xi_x - \cos \theta \right], \quad (2.9b)$$

$$\frac{dV_y}{dT} = -\alpha \left[V_y - \sqrt{2\kappa D_t} \xi_y - \sin \theta \right], \quad (2.9c)$$

$$\frac{d\chi}{dT} = -\beta \left[\chi - 4V_f Y - \sqrt{2\kappa D_r} \eta - \mathcal{M} \right], \quad (2.9d)$$

where

$$\alpha = \frac{\kappa}{\tau}, \quad \beta = \frac{\kappa}{\tau_R}$$

are dimensionless parameters corresponding to translational and rotational inertia of the particle respectively with $\kappa = L/v_0$ being the ratio of channel height to particle's self-propulsion speed.

2.2 Numerical simulation framework

We adopt the numerical simulation approach described in [99, 102] to approximate the continuous-time solution $[X(T), Y(T), \theta(T), V_x(T), V_y(T), \chi(T)]$ of the dimensionless stochastic differential equations given by Eqn. (2.9). The discrete time-sequence $[X_i, Y_i, \theta_i, V_{x,i}, V_{y,i}, \chi_i]$, which approximates the continuous solution, is evaluated at regular time steps $T_i = i\Delta T$, where ΔT is a sufficiently small time step.

2.2.1 Finite difference equations

Explicitly, the set of finite difference equations can be obtained from Eqn. (2.9) by carrying out the following substitutions:

$$X \rightarrow X_i, \quad Y \rightarrow Y_i, \quad \theta \rightarrow \theta_i; \quad (2.10a)$$

$$V_x \rightarrow V_{x,i}, \quad V_y \rightarrow V_{y,i}, \quad \chi \rightarrow \chi_i; \quad (2.10b)$$

$$\frac{dX}{dT} = \frac{X_{i+1} - X_i}{\Delta T}, \quad \frac{dY}{dT} = \frac{Y_{i+1} - Y_i}{\Delta T}, \quad \frac{d\theta}{dT} = \frac{\theta_{i+1} - \theta_i}{\Delta T}; \quad (2.10c)$$

$$\frac{dV_x}{dT} = \frac{V_{x,i+1} - V_{x,i}}{\Delta T}, \quad \frac{dV_y}{dT} = \frac{V_{y,i+1} - V_{y,i}}{\Delta T}, \quad \frac{d\chi}{dT} = \frac{\chi_{i+1} - \chi_i}{\Delta T}; \quad (2.10d)$$

$$\xi_x = \frac{w_{x,i}}{\sqrt{\Delta T}}, \quad \xi_y = \frac{w_{y,i}}{\sqrt{\Delta T}}, \quad \eta = \frac{w_{\theta,i}}{\sqrt{\Delta T}}. \quad (2.10e)$$

(2.10)

Here $w_{x,i}$, $w_{y,i}$, and $w_{\theta,i}$ are uncorrelated sequences of random numbers taken from a Gaussian distribution with zero mean and standard deviation 1. Many programming languages have built-in functions that directly generate such random sequences, such as the

`randn()` function in MATLAB. Alternatively, it is possible to generate Gaussian random numbers from uniform random numbers between 0 and 1 using various techniques such as the Box-Müller algorithm or the Marsaglia polar algorithm. The numerical solution is then obtained by solving the resulting finite difference equation recursively for $[X_{i+1}, Y_{i+1}, \theta_{i+1}, V_{x,i+1}, V_{y,i+1}, \chi_{i+1}]$ using the values $[X_i, Y_i, \theta_i, V_{x,i}, V_{y,i}, \chi_i]$ obtained from the previous iteration:

$$X_{i+1} = X_i + V_{x,i}\Delta T, \quad (2.11a)$$

$$Y_{i+1} = Y_i + V_{y,i}\Delta T, \quad (2.11b)$$

$$\theta_{i+1} = \theta_i + \chi_i\Delta T, \quad (2.11c)$$

$$V_{x,i+1} = V_{x,i} - \alpha\Delta T \left[V_{x,i} - V_f(1 - 4Y_i^2) - \sqrt{2\kappa D_t/\Delta T} w_{x,i} - \cos \theta_i \right], \quad (2.11d)$$

$$V_{y,i+1} = V_{y,i} - \alpha\Delta T \left[V_{y,i} - \sqrt{2\kappa D_t/\Delta T} w_{y,i} - \sin \theta_i \right], \quad (2.11e)$$

$$\chi_{i+1} = \chi_i - \beta\Delta T \left[\chi_i - 4V_f Y_i - \sqrt{2\kappa D_r/\Delta T} w_{\theta,i} - \mathcal{M} \right]. \quad (2.11f)$$

We note that this is a first-order integration method that generalizes the Euler method to stochastic differential equations; higher-order algorithms can also be employed to obtain faster convergence of the solution. The finite difference equations of the dimensional equations of motion, given by Eqn. (2.8), can be obtained by proceeding in a similar manner as above.

2.2.2 Reflective boundaries

When self-propelled particles move through a patterned environment, frequent encounters with obstacles will occur, for example, encounters with the walls of a microchannel. Whenever an active particle contacts an obstacle, it slides along the obstacle until its orientation points away from it. Numerically, this process can be modelled using reflective boundaries [99], as shown in Fig. 2.1. Note that, in this approach, the orientation of the particle θ is assumed to remain unchanged.

The concrete implementation of the reflective boundary condition is realized by updating each time step the particle position from $\mathbf{r}_{i-1} = (x_{i-1}, y_{i-1})$ to $\mathbf{r}_i = (x_i, y_i)$ according to the following algorithm:

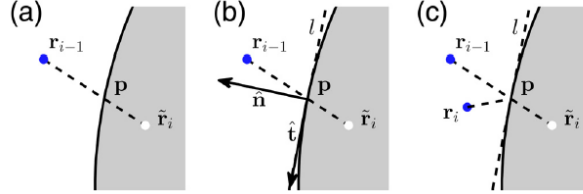


Figure 2.1: Implementation of reflective boundary conditions. At each time step, the algorithm (a) checks whether a particle has moved inside an obstacle; if so: (b) the boundary of the obstacle is approximated by its tangent l at the point \mathbf{p} where the particle entered the obstacle, and (c) the particle position is reflected on this line. Reproduced from [99].

1. Tentatively update the particle position to $\tilde{\mathbf{r}}_i = (\tilde{x}_i, \tilde{y}_i)$ according to Eqn. (2.11);
2. If $\tilde{\mathbf{r}}_i$ is not inside any obstacle, set $\mathbf{r}_i = \tilde{\mathbf{r}}_i$ and move on to the next time step;
3. Otherwise, if $\tilde{\mathbf{r}}_i$ is inside some obstacle, as depicted in Fig. 2.1(a):
 - (a) Find the intersection point $\mathbf{p} = (x_p, y_p)$ between the boundary and the straight line from \mathbf{r}_{i-1} to $\tilde{\mathbf{r}}_i$;
 - (b) Find the equation of the tangent l to the obstacle at \mathbf{p} with tangent unit vector $\hat{\mathbf{t}}$ and normal unit vector $\hat{\mathbf{n}}$ (outgoing from the obstacle), as shown in Fig. 2.1(b);
 - (c) Find \mathbf{r}_i by reflecting $\tilde{\mathbf{r}}_i$ on l (assuming l to be a mirror), so that

$$\mathbf{r}_i = \tilde{\mathbf{r}}_i - 2[(\tilde{\mathbf{r}}_i - \mathbf{p}) \cdot \hat{\mathbf{n}}] \hat{\mathbf{n}}, \quad (2.12)$$

where $(\tilde{\mathbf{r}}_i - \mathbf{p}) \cdot \hat{\mathbf{n}}$ is the (shortest) distance between $\tilde{\mathbf{r}}_i$ and l .

The crucial condition for this numerical approach to work is that the average spatial increment of the simulated trajectory, i.e. $\langle \Delta x_i \rangle$ and $\langle \Delta y_i \rangle$ for 2D simulation, is small compared to the characteristic length scale of the obstacles. This approach restricts one to consider only one boundary at a time and also to approximate the boundary with the tangent line to the boundary at the intersection point. If the time step Δt is too large, this approach can lead to some numerical instability around sharp corners in the boundaries, where multiple reflections may take place (due to multiple tangents at the intersection point), or on an obstacle wall that is too thin, where the particle's trajectory could unnaturally pass through the obstacle.

In our numerical simulations, we are interested in microchannels and hence the only obstacles that we care about are the plane horizontal walls of the channel located at $y = \pm L/2$.

In this case, step (2) reduces to checking if $|\tilde{y}_i| > L/2$ ($|\tilde{Y}_i| > 0.5$ in non-dimensional form); if false, then we set $(x_i, y_i) = (\tilde{x}_i, \tilde{y}_i)$ and move on to the next time step, if true, then according to step (3.c), we set

$$[x_i, y_i] = [\tilde{x}_i, \operatorname{sgn}(\tilde{y}_i)(L - |\tilde{y}_i|)]. \quad (2.13)$$

In non-dimensional form, we set

$$[X_i, Y_i] = [\tilde{X}_i, \operatorname{sgn}(\tilde{Y}_i)(1 - |\tilde{Y}_i|)]. \quad (2.14)$$

2.3 Inertialess equations of motion

If we consider the particle under consideration to be inertialess, then the mass of the particle $m \approx 0$, which in turn implies that the moment of inertia of the particle $J \approx 0$. Therefore, in this case, substituting $m = 0$ and $J = 0$ in Eqns. (2.5b) and (2.6b) respectively, the equations of motion read as follows:

$$\dot{\mathbf{r}} = \mathbf{v} = \mathbf{v}_f + \sqrt{2D_T}\boldsymbol{\xi} + v_0\mathbf{n}, \quad (2.15a)$$

$$\dot{\theta} = \omega = \omega_s + \sqrt{2D_R}\eta + \Omega. \quad (2.15b)$$

(2.15)

In terms of components, the above equations can be written as follows:

$$\frac{dx}{dt} = v_f \left(1 - \frac{4y^2}{L^2}\right) + \sqrt{2D_T}\xi_x + v_0 \cos \theta, \quad (2.16a)$$

$$\frac{dy}{dt} = \sqrt{2D_T}\xi_y + v_0 \sin \theta, \quad (2.16b)$$

$$\frac{d\theta}{dt} = \frac{4v_f y}{L^2} + \sqrt{2D_R}\eta + \Omega. \quad (2.16c)$$

2.3.1 Non-dimensionalisation

Adopting the same non-dimensionalisation as before, Eqn. (2.16) can be written in its dimensionless form as follows:

$$\frac{dX}{dT} = V_f(1 - 4Y^2) + \sqrt{2\kappa D_t} \xi_x + \cos \theta, \quad (2.17a)$$

$$\frac{dY}{dT} = \sqrt{2\kappa D_t} \xi_y + \sin \theta. \quad (2.17b)$$

$$\frac{d\theta}{dT} = 4V_f Y + \sqrt{2\kappa D_r} \eta + \mathcal{M}. \quad (2.17c)$$

2.3.2 Finite difference equations

To obtain the finite difference equations corresponding to Eqn. (2.17), we make substitutions as given by Eqn. (2.10):

$$X_{i+1} = X_i + \Delta T \left[V_f(1 - 4Y_i^2) + \sqrt{2\kappa D_t / \Delta T} w_{x,i} + \cos \theta \right], \quad (2.18a)$$

$$Y_{i+1} = Y_i + \Delta T \left[\sqrt{2\kappa D_t / \Delta T} w_{y,i} + \sin \theta \right], \quad (2.18b)$$

$$\theta_{i+1} = \theta_i + \Delta T \left[4V_f Y_i + \sqrt{2\kappa D_r / \Delta T} w_{\theta,i} + \mathcal{M} \right]. \quad (2.18c)$$

Chapter 3

Results and discussions

3.1 Trajectories and phase spaces

By employing the numerical simulation framework presented in Section 2.2, one can obtain and scrutinize the two-dimensional trajectories and phase spaces of an active Brownian particle in a microchannel with Poiseuille flow, using MATLAB or any other appropriate simulation software. The trajectory of a non-inertial active particle can be determined by employing the FDEs in Eqn. (2.18), whereas the trajectory of an inertial active particle can be obtained by implementing the FDEs in Eqn. (2.11).

We first investigate the trajectories of a non-inertial active particle and three inertial active particles with mass $m = 1.5 \times 10^{-10}$ kg (*Inertial S3*), $m = 1.5 \times 10^{-9}$ kg (*Inertial S2*), and $m = 1.5 \times 10^{-8}$ kg (*Inertial S1*) under various temperature and flow speed conditions. The trajectories are shown in Fig. 3.1, with an initial condition $(X_0, Y_0, \theta_0) = (0, 0, \pi/6)$. Figs. 3.1a, 3.1b, and 3.1c depict the noise-free trajectories at flow speeds $V_f = 0.28$, $V_f = 2.25$, and $V_f = 6.75$, respectively, at a temperature of 0K, where both translational and rotational diffusion coefficients are zero ($D_t = D_r = 0$). In contrast, the other figures in Fig. 3.1 represent trajectories at higher temperatures with varying flow speeds.

The results show that the increase in temperature and flow speed leads to more random and chaotic trajectories of active Brownian particles. However, the level of chaos decreases with an increase in particle mass, with the least chaotic trajectories observed in the particle with the highest mass (*Inertial S1*). The particle with the least mass (*Inertial S3*) shows a trajectory that approximates that of a non-inertial particle, indicating the dominance of non-inertial effects in its dynamics. *Inertial S1* and *Inertial S2* move slower than *Inertial*

S3 and the non-inertial active particle, requiring more time to reorient upon collision with the walls or due to collisions with the surrounding medium particles. Consequently, they spend more time near the channel walls than in the center of the microchannel.

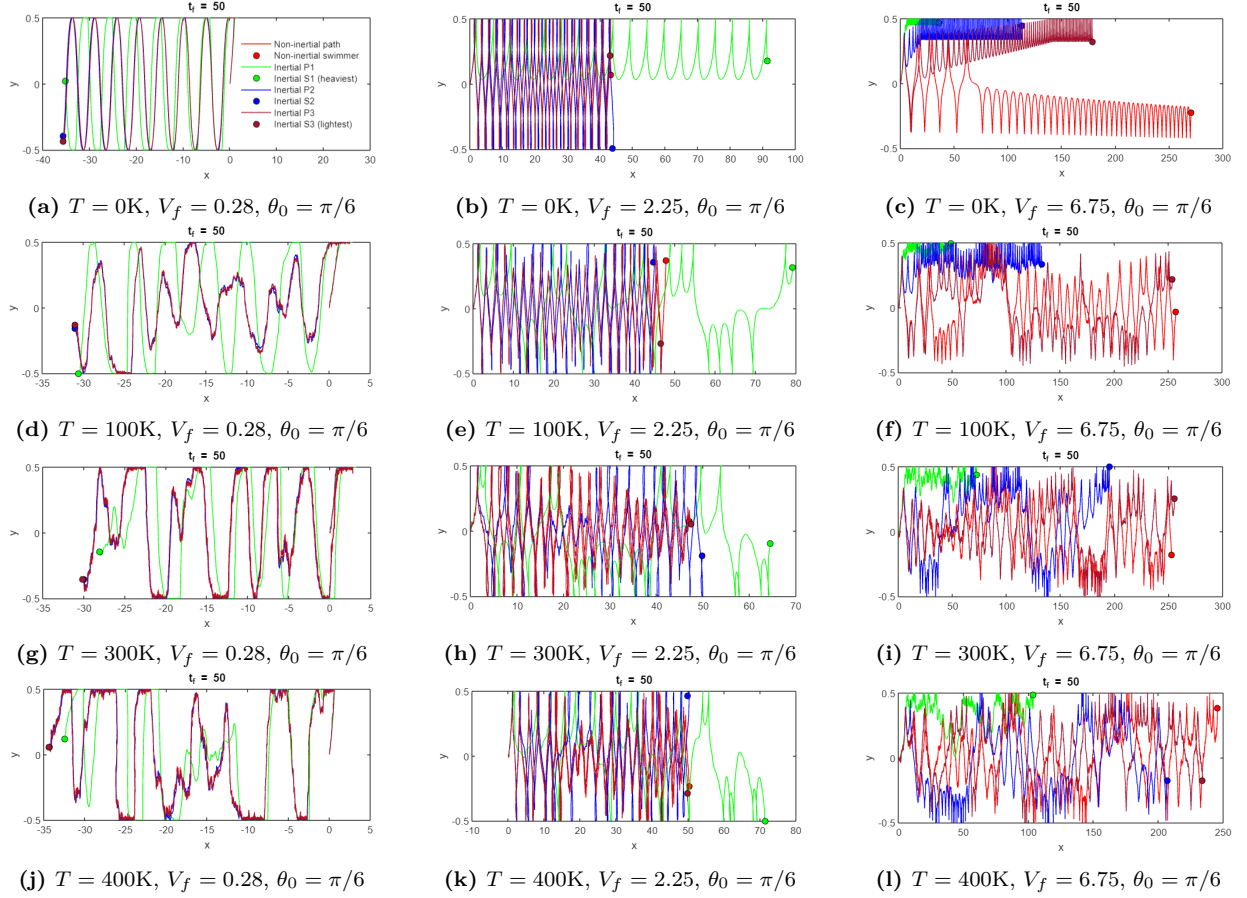
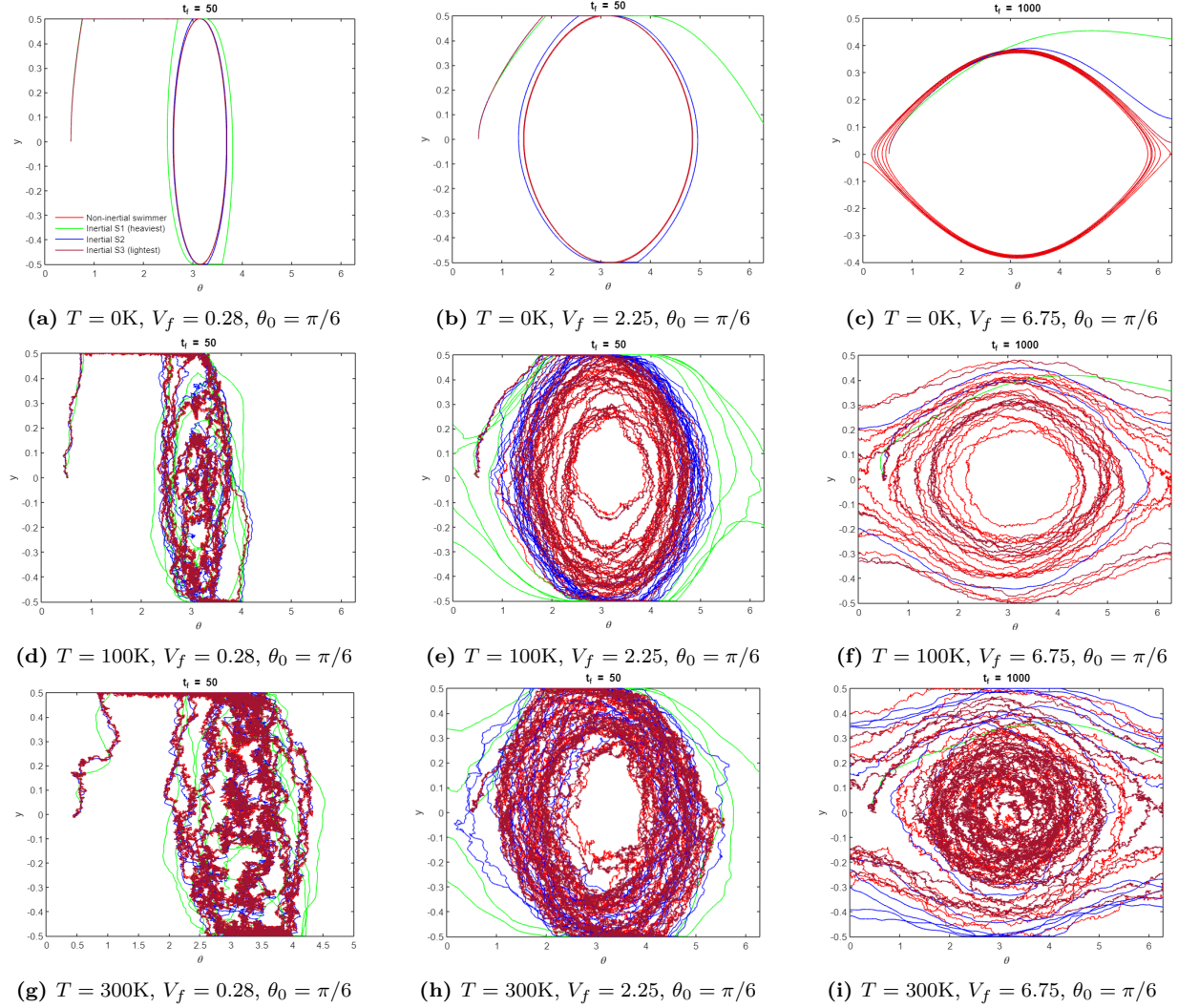


Figure 3.1: Trajectories of four active Brownian particles with different masses in a microchannel with Poiseuille flow, subjected to varying non-dimensional flow speeds and temperatures. The trajectories, colored red (Non-inertial path), green (Inertial P1), blue (Inertial P2), and dark red (Inertial P3), correspond to the non-inertial particle and particles with mass $m = 1.5 \times 10^{-8}$ kg (Inertial S1), $m = 1.5 \times 10^{-9}$ kg (Inertial S2), and $m = 1.5 \times 10^{-10}$ kg (Inertial S3), respectively. The initial condition for all trajectories is $(X_0, Y_0, \theta_0) = (0, 0, \pi/6)$.

In addition to the trajectories of active Brownian particles, phase spaces or $Y\text{-}\theta$ plots are a useful tool for understanding the dynamics of such particles. The phase spaces of a non-inertial active particle and three inertial active particles, Inertial S3, Inertial S2, and Inertial S1, are presented in Fig. 3.2, depicting their behavior under varying temperature and flow

speed conditions. These plots provide valuable insights into the orientation and movement of active Brownian particles in microchannels, and how their dynamics are influenced by inertia. The information obtained from the phase spaces can be used to analyze the motion of active Brownian particles in confined spaces and to develop strategies for controlling their movement.



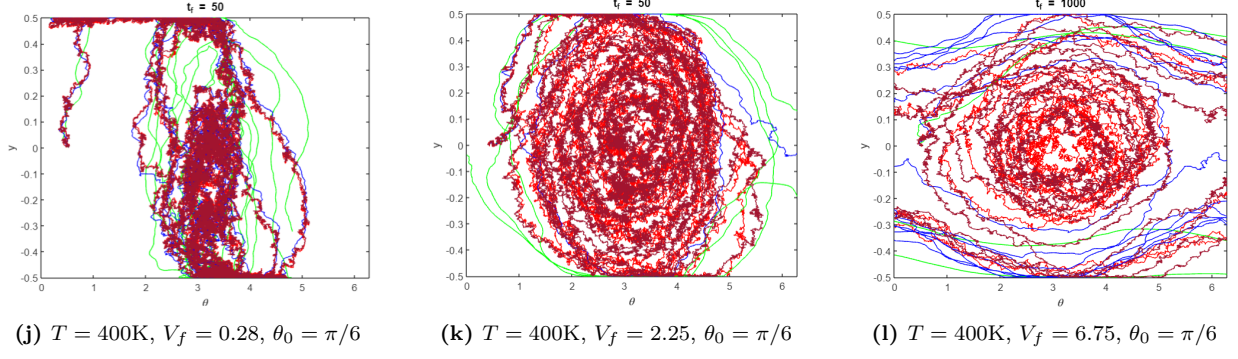


Figure 3.2: Phase portraits of four active Brownian particles with different masses in a microchannel with Poiseuille flow, under varying non-dimensional flow speeds and temperatures. The red, green, blue, and dark red plots correspond to the non-inertial particle and particles with masses of 1.5×10^{-8} kg (Inertial S1), 1.5×10^{-9} kg (Inertial S2), and 1.5×10^{-10} kg (Inertial S3), respectively. The initial condition for all the plots is $(X_0, Y_0, \theta_0) = (0, 0, \pi/6)$.

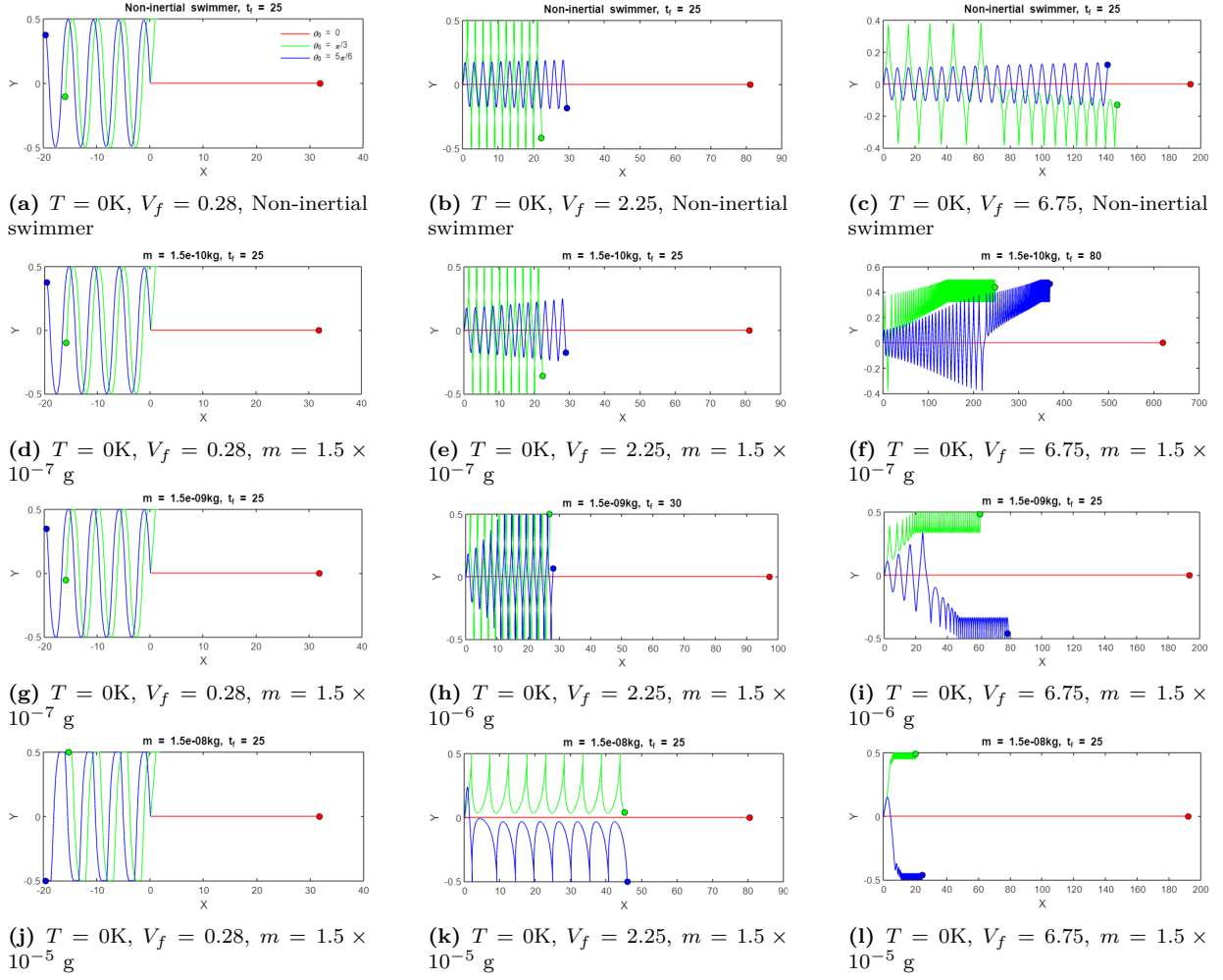
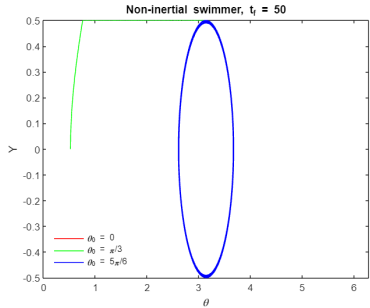
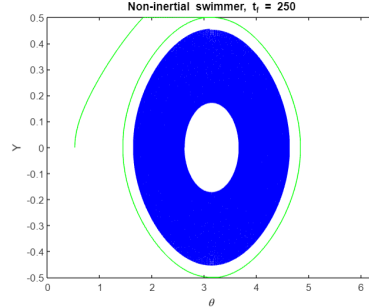


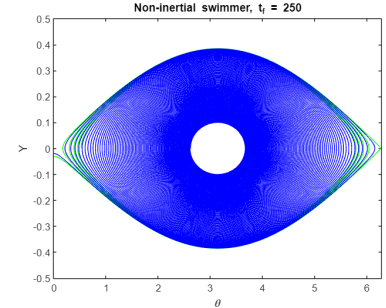
Figure 3.3: Trajectories of four active Brownian particles with different masses in a microchannel with Poiseuille flow under varying non-dimensional flow speeds and initial orientations. The red, green, and blue trajectories correspond to the initial orientation $\theta_0 = 0$, $\theta_0 = \pi/6$, and $\theta_0 = 5\pi/6$, respectively. All trajectories have an initial position of $(X_0, Y_0) = (0, 0)$ and are at temperature 0K.



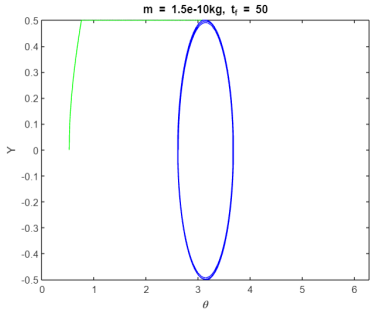
(a) $T = 0\text{K}$, $V_f = 0.28$, Non-inertial swimmer



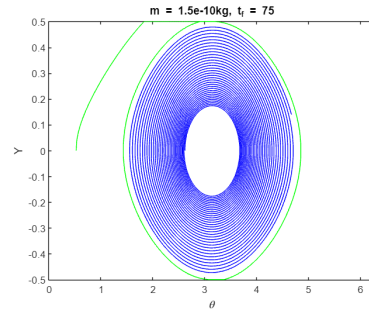
(b) $T = 0\text{K}$, $V_f = 2.25$, Non-inertial swimmer



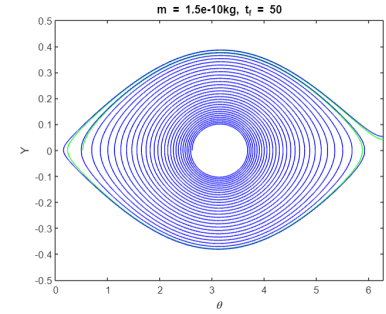
(c) $T = 0\text{K}$, $V_f = 6.75$, Non-inertial swimmer



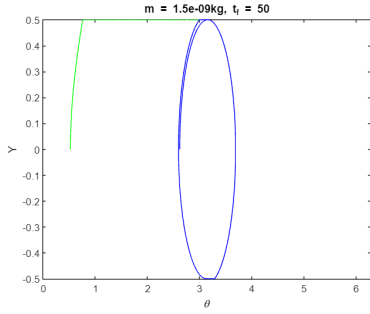
(d) $T = 0\text{K}$, $V_f = 0.28$, $m = 1.5 \times 10^{-7} \text{ g}$



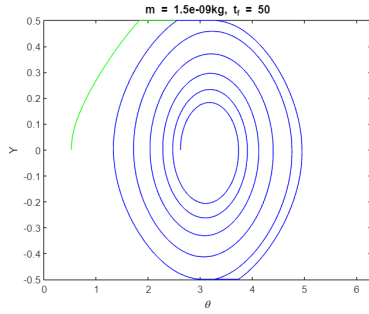
(e) $T = 0\text{K}$, $V_f = 2.25$, $m = 1.5 \times 10^{-7} \text{ g}$



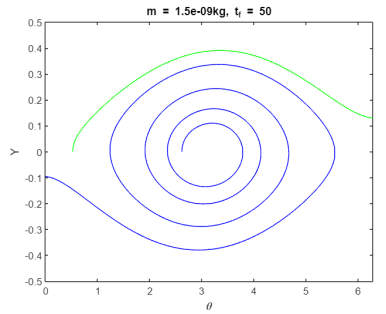
(f) $T = 0\text{K}$, $V_f = 6.75$, $m = 1.5 \times 10^{-7} \text{ g}$



(g) $T = 0\text{K}$, $V_f = 0.28$, $m = 1.5 \times 10^{-6} \text{ g}$



(h) $T = 0\text{K}$, $V_f = 2.25$, $m = 1.5 \times 10^{-6} \text{ g}$



(i) $T = 0\text{K}$, $V_f = 6.75$, $m = 1.5 \times 10^{-6} \text{ g}$

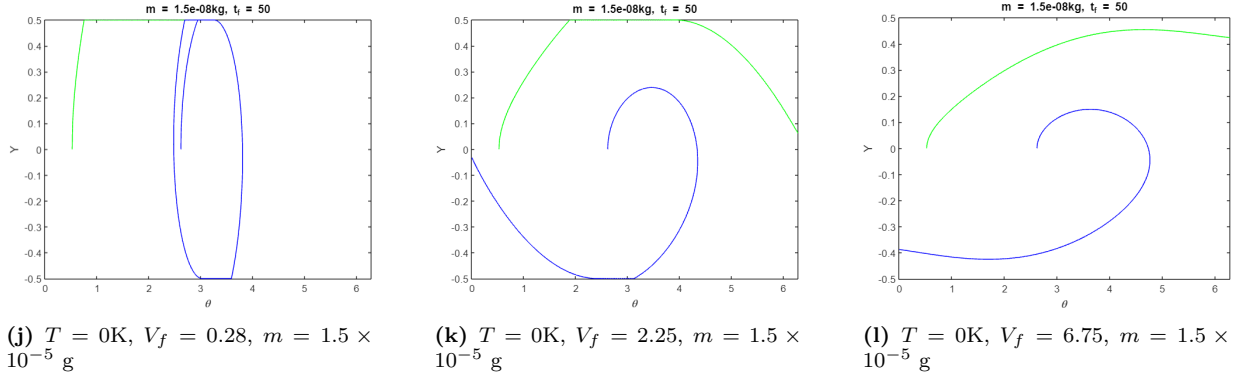


Figure 3.4: Phase portraits of four active Brownian particles with different masses in a microchannel with Poiseuille flow under varying non-dimensional flow speeds and initial orientations. The red, green, and blue plots correspond to the initial orientation $\theta_0 = 0$, $\theta_0 = \pi/6$, and $\theta_0 = 5\pi/6$, respectively. All plots have an initial position of $(X_0, Y_0) = (0, 0)$ and are at temperature 0K.

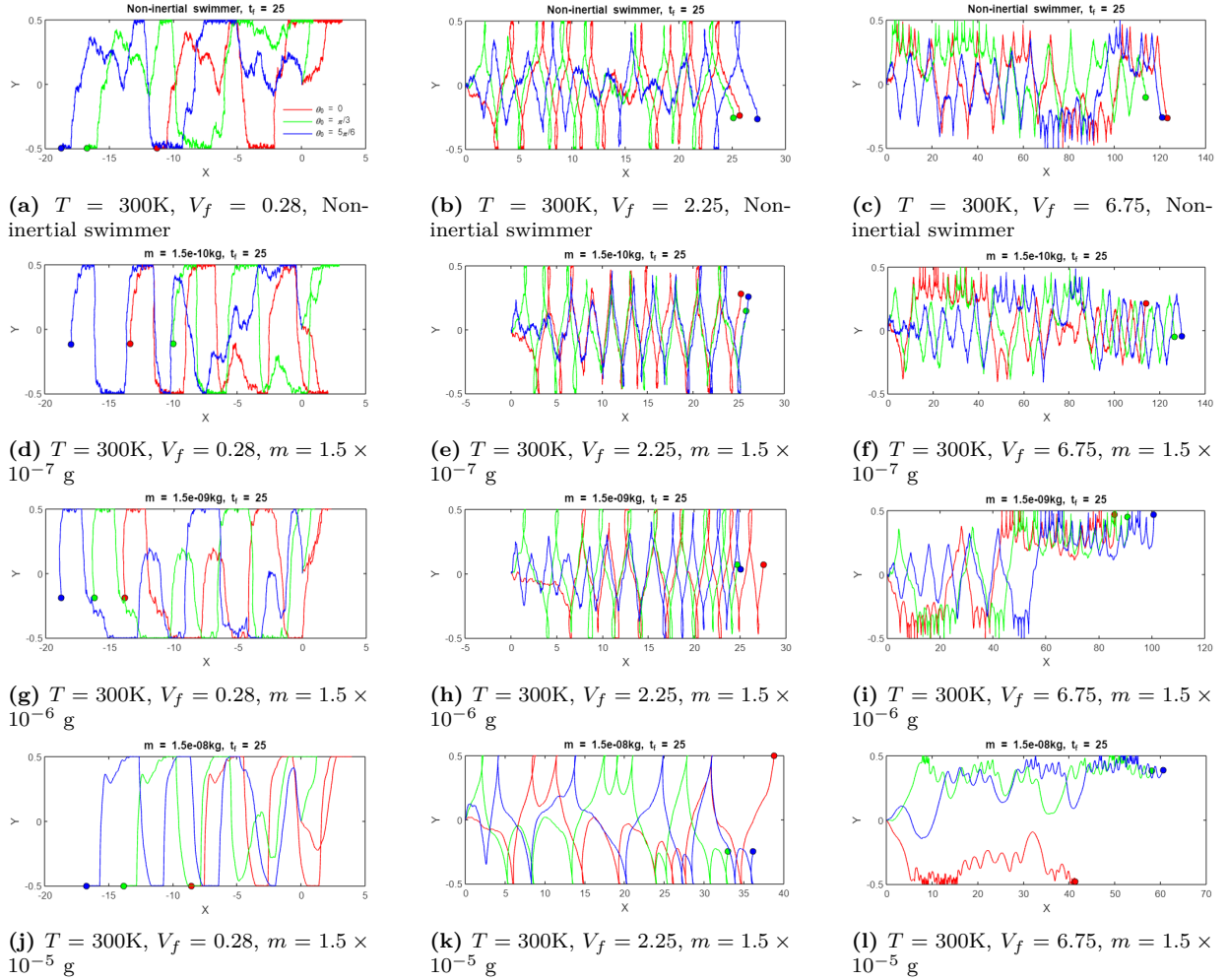
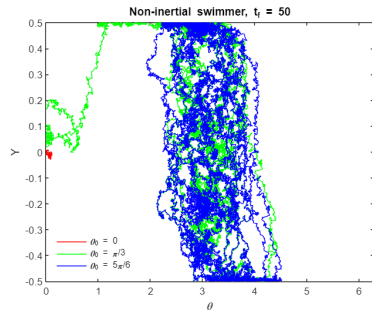
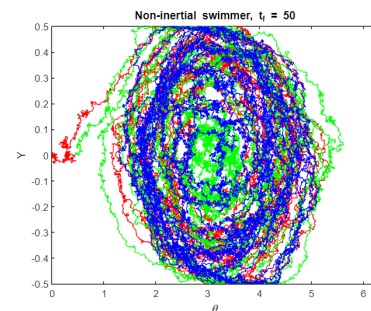


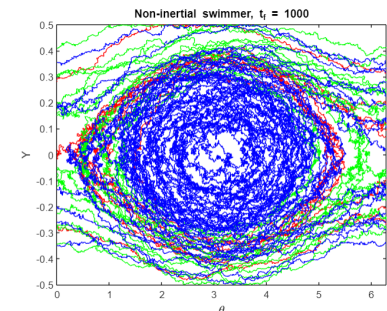
Figure 3.5: Trajectories of four active Brownian particles with different masses in a microchannel with Poiseuille flow under varying non-dimensional flow speeds and initial orientations. The red, green, and blue trajectories correspond to the initial orientation $\theta_0 = 0$, $\theta_0 = \pi/6$, and $\theta_0 = 5\pi/6$, respectively. All trajectories have an initial position of $(X_0, Y_0) = (0, 0)$ and are at temperature 300K.



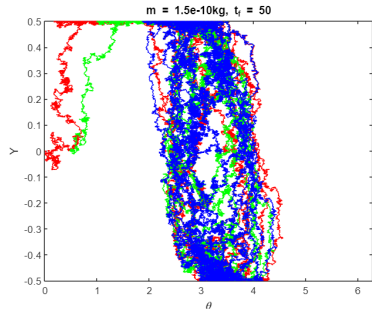
(a) $T = 300K$, $V_f = 0.28$, Non-inertial swimmer



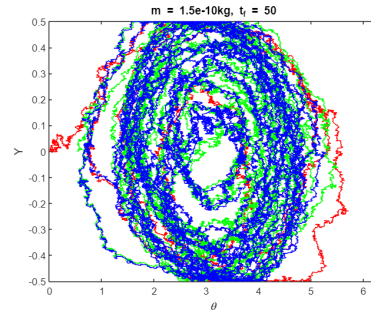
(b) $T = 300K$, $V_f = 2.25$, Non-inertial swimmer



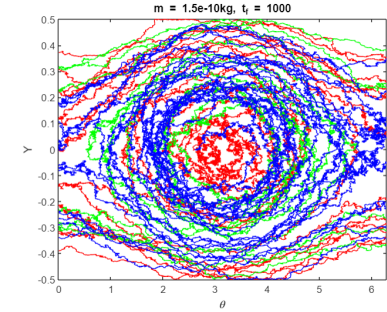
(c) $T = 300K$, $V_f = 6.75$, Non-inertial swimmer



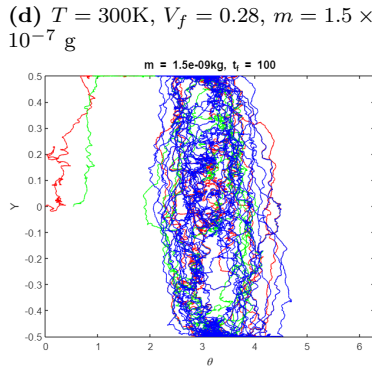
(d) $T = 300K$, $V_f = 0.28$, $m = 1.5 \times 10^{-7} g$



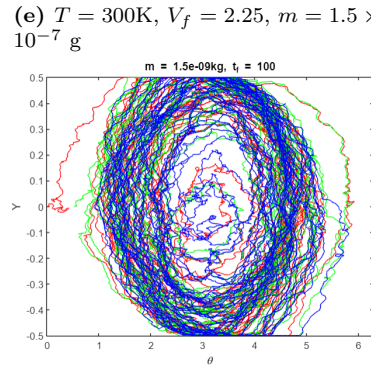
(e) $T = 300K$, $V_f = 2.25$, $m = 1.5 \times 10^{-7} g$



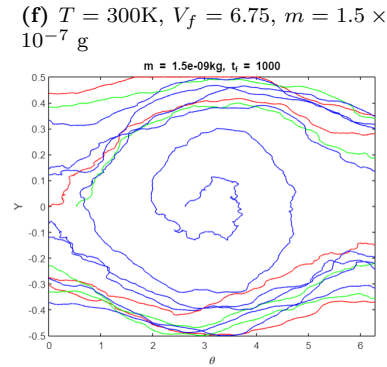
(f) $T = 300K$, $V_f = 6.75$, $m = 1.5 \times 10^{-7} g$



(g) $T = 300K$, $V_f = 0.28$, $m = 1.5 \times 10^{-6} g$



(h) $T = 300K$, $V_f = 2.25$, $m = 1.5 \times 10^{-6} g$



(i) $T = 300K$, $V_f = 6.75$, $m = 1.5 \times 10^{-6} g$

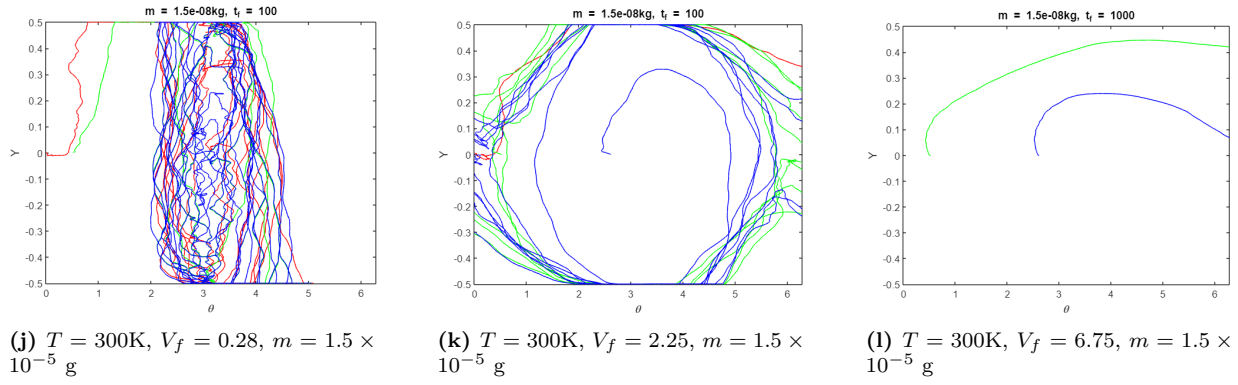


Figure 3.6: Phase portraits of four active Brownian particles with different masses in a microchannel with Poiseuille flow under varying non-dimensional flow speeds and initial orientations. The red, green, and blue plots correspond to the initial orientation $\theta_0 = 0$, $\theta_0 = \pi/6$, and $\theta_0 = 5\pi/6$, respectively. All plots have an initial position of $(X_0, Y_0) = (0, 0)$ and are at temperature 300K.

3.2 Statistical analysis

In order to gain a deeper understanding of the statistical mechanics of a self-propelled Brownian particle with inertia, we conduct a statistical analysis by examining key statistical quantities that can be derived from the particle's trajectories and phase spaces. These quantities include the mean squared displacement (MSD), velocity autocorrelation function (VACF), and joint probability distribution function (joint PDF or JPDF). By comparing these quantities for inertial and non-inertial particles, we aim to identify differences in their statistical behavior and gain insights into the effects of inertia on the particle dynamics.

3.2.1 Mean squared displacement (MSD)

The MSD is a statistical quantity that quantifies how a collection of particles move from its initial position. For any collection of N particles, the mean squared displacement at any time $t \geq 0$ is defined as an ensemble average:

$$\text{MSD}(t) = \left\langle |\mathbf{r}(t) - \mathbf{r}(0)|^2 \right\rangle = \frac{1}{N} \sum_{i=1}^N |\mathbf{r}^{(i)}(t) - \mathbf{r}^{(i)}(0)|^2, \quad (3.1)$$

where $\mathbf{r}^{(i)}(0)$ is the initial position of the i -th particle and $\mathbf{r}^{(i)}(t)$ is the position of the i -th particle at time t .

Note that, in ergodic systems, the time average of a quantity coincides with the ensemble average, i.e., the average over all possible configurations, which, in the case of the motion of a particle, are all possible realisation of a trajectory. Hence, or otherwise according to [99, 102, 103], given the trajectory (x, y) of a moving particle, the MSD at any time $\tau_1 \geq 0$ is given by the time average

$$\begin{aligned} \text{MSD}(\tau_1) &= \left\langle |\mathbf{r}(t + \tau_1) - \mathbf{r}(t)|^2 \right\rangle \\ &= \frac{1}{T_1 - \tau_1} \int_0^{T_1 - \tau_1} |\mathbf{r}(t + \tau_1) - \mathbf{r}(t)|^2 dt, \end{aligned} \quad (3.2)$$

where T_1 is the final observation time. Thus, from Eqn. (3.2), it may be noted that the MSD over a given time τ represents the average quadratic displacement from the position the particle had a time τ before. Considering a 2D motion, Eqn. (3.2) becomes

$$\text{MSD}(\tau_1) = \frac{1}{T_1 - \tau_1} \int_0^{T_1 - \tau_1} [\{x(t + \tau_1) - x(t)\}^2 + \{y(t + \tau_1) - y(t)\}^2] dt. \quad (3.3)$$

Thus, given a 2D trajectory sequence $[x_i, y_i]$ of a particle, sampled at discrete times t_i with a time step Δt , the MSD can be calculated as follows:

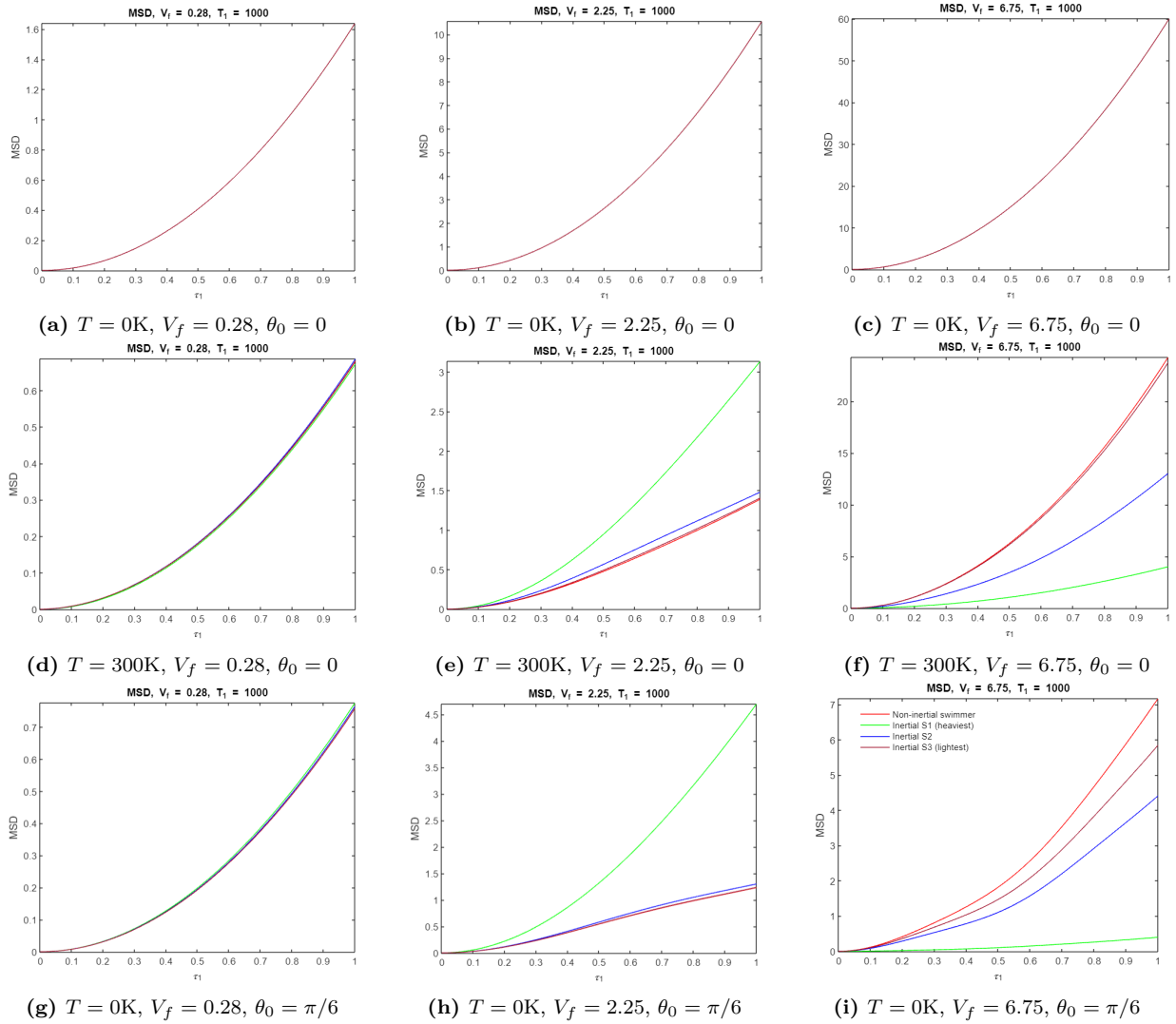
$$\begin{aligned} \text{MSD}_{j+1} &= \text{MSD}(j\Delta t) \\ &= \left\langle \left[(x_{i+j} - x_i)^2 + (y_{i+j} - y_i)^2 \right] \right\rangle \\ &= \frac{1}{n-j} \sum_{i=1}^{n-j} \left[(x_{i+j} - x_i)^2 + (y_{i+j} - y_i)^2 \right], \end{aligned} \quad (3.4)$$

for all integers $0 \leq j \leq N$, where $n = \frac{T_1}{\Delta t} + 1$ and usually, $N = \lfloor \sqrt{n} \rfloor$.

The MSD of an inertialess active Brownian particle in an unbounded fluid, i.e., for a trajectory governed by Eqn. (2.16) without any boundary conditions, is given by

$$\text{MSD}(\tau_1) = (4D_T + v_0^2\tau_P)\tau_1 + \frac{v_0^2\tau_P^2}{2} \left(e^{-\frac{2\tau_1}{\tau_P}} - 1 \right). \quad (3.5)$$

Fig. 3.7 illustrates the MSD-time (τ_1) plots of the four self-propelled Brownian particles, including the non-inertial active particle, Inertial S3, Inertial S2, and Inertial S1, under varying flow speeds, temperatures, and initial conditions. These plots were obtained using MATLAB, utilizing the equation for mean squared displacement (MSD) given by Eqn. (3.4). The MSD-time plots offer valuable insights into the degree of randomness and diffusivity of the particles, making them a useful tool for studying their dynamics. These plots provide crucial information for understanding the behavior of the particles and offer a basis for developing models to control their motion and transport in confined spaces.



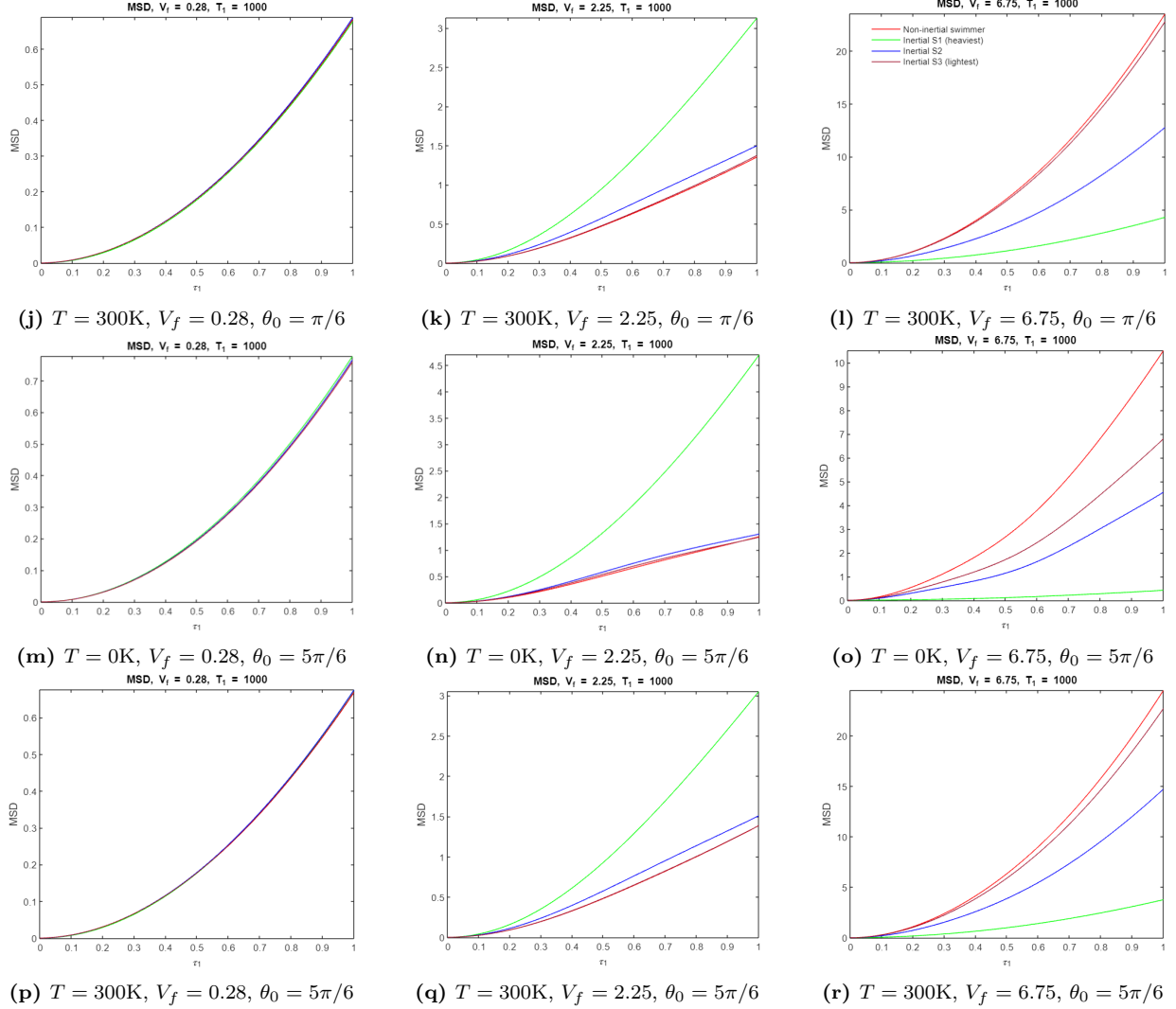


Figure 3.7: MSD as a function of time (τ_1) depicted by $\text{MSD} - \tau_1$ plots for four active Brownian particles with different masses in a microchannel with Poiseuille flow, under varying non-dimensional flow speeds, temperatures, and initial orientations. The plots colored red, green, blue, and dark red correspond to the non-inertial particle and particles with masses of $1.5 \times 10^{-8} \text{ kg}$ (Inertial S1), $1.5 \times 10^{-9} \text{ kg}$ (Inertial S2), and $1.5 \times 10^{-10} \text{ kg}$ (Inertial S3), respectively. The initial position for all the plots is $(X_0, Y_0) = (0, 0)$.

3.2.2 Velocity autocorrelation function (VACF)

For a self-propelled Brownian particle, the velocity autocorrelation function (VACF) is a measure of how quickly the particle forgets its initial velocity. At any time $\tau_1 \geq 0$, for the motion of the particle in two dimensions, it is defined as

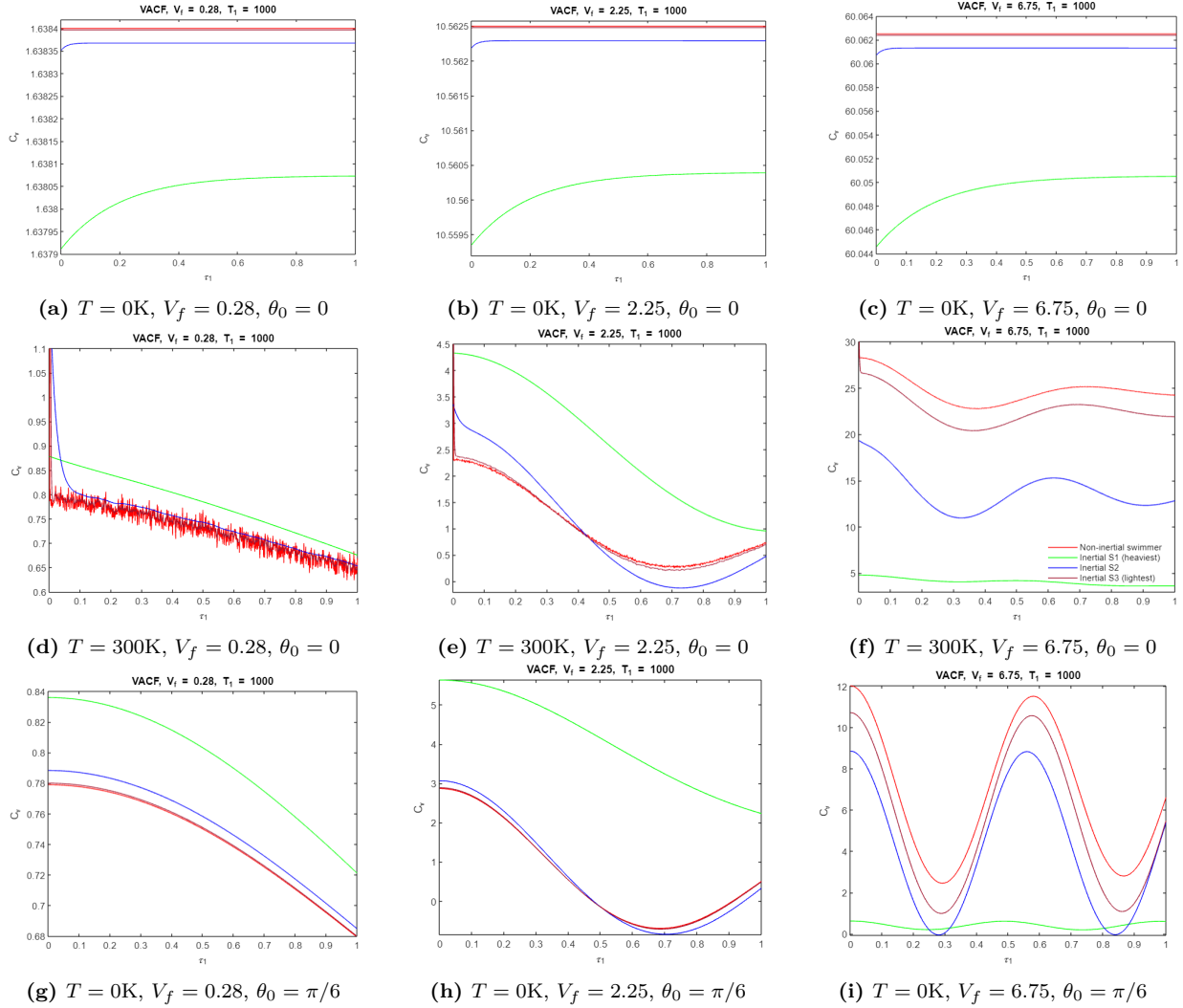
$$\begin{aligned} C_v(\tau_1) &= \langle \mathbf{v}(t + \tau_1) \cdot \mathbf{v}(t) \rangle \\ &= \langle v_x(t + \tau_1)v_x(t) + v_y(t + \tau_1)v_y(t) \rangle \\ &= \frac{1}{T_1 - \tau_1} \int_0^{T_1 - \tau_1} [v_x(t + \tau_1)v_x(t) + v_y(t + \tau_1)v_y(t)] dt, \end{aligned} \quad (3.6)$$

where $\mathbf{v} = (v_x, v_y)$ is the velocity of the particle and T_1 is the final observation time. Numerically, similar to the numerical expression for MSD, VACF is given by

$$\begin{aligned} C_{v,j+1} &= C_v(j\Delta t) \\ &= \langle v_{x,i+j}v_{x,i} + v_{y,i+j}v_{y,i} \rangle \\ &= \frac{1}{n-j} \sum_{i=1}^{n-j} (v_{x,i+j}v_{x,i} + v_{y,i+j}v_{y,i}), \end{aligned} \quad (3.7)$$

for all integers $0 \leq j \leq N$, where $n = \frac{T_1}{\Delta t} + 1$ and usually, $N = \lfloor \sqrt{n} \rfloor$.

The velocity autocorrelation function (C_v) plotted against time (τ_1) for the four self-propelled Brownian particles, namely, the non-inertial active particle, Inertial S3, Inertial S2, and Inertial S1, are displayed in Fig. 3.8. These plots were generated using MATLAB and the equation for VACF given by Eqn. (3.7) (or other appropriate discrete algorithms). The VACF-time plots provide information on the correlation between the velocity of the particles at different times and offer a useful tool to study the dynamics of the particles. These plots can be used to analyze the persistence of motion and to determine the degree of correlation between the velocities of the particles at different times.



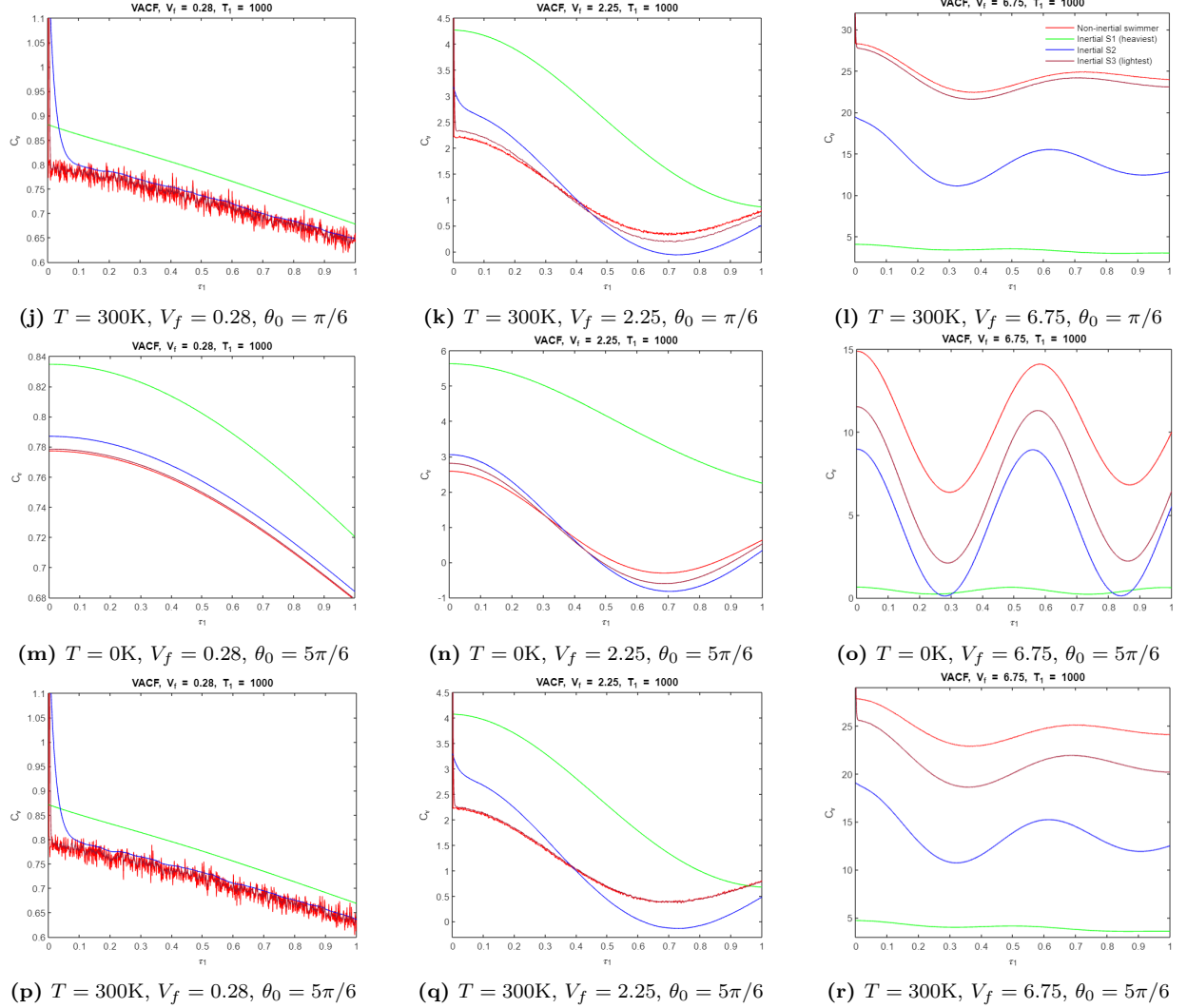
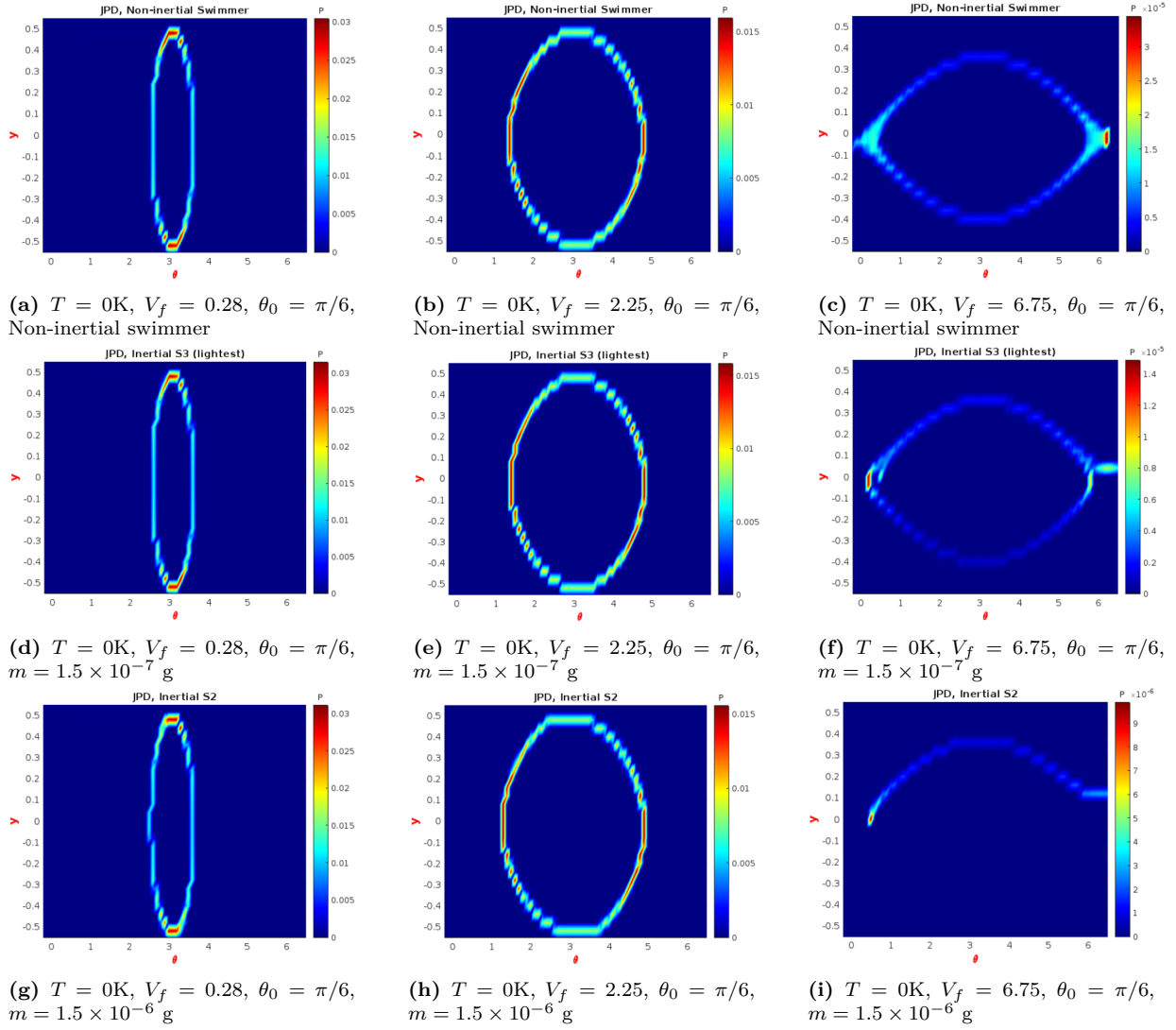


Figure 3.8: VACF (C_v) as a function of time (τ_1) depicted by $C_v - \tau_1$ plots for four active Brownian particles with different masses in a microchannel with Poiseuille flow, under varying non-dimensional flow speeds, temperatures, and initial orientations. The plots colored red, green, blue, and dark red correspond to the non-inertial particle and particles with masses of 1.5×10^{-8} kg (Inertial S1), 1.5×10^{-9} kg (Inertial S2), and 1.5×10^{-10} kg (Inertial S3), respectively. The initial position for all the plots is $(X_0, Y_0) = (0, 0)$.

3.2.3 Joint probability distribution function (JPDF) of the phase space

In the context of active Brownian particles, the joint probability distribution function (JPDF) of the phase space variables provides important information about the statistical behavior of the particles. The JPDF of the phase space variables, Y and θ , can be obtained by computing the probability density function of Y and θ at each point in the phase space and plotting it as a two-dimensional histogram. The JPDF can be used to study the correlation between the orientation and the position of the particles in the microchannel, and to understand how changes in the flow conditions and temperature affect the behavior of the particles.



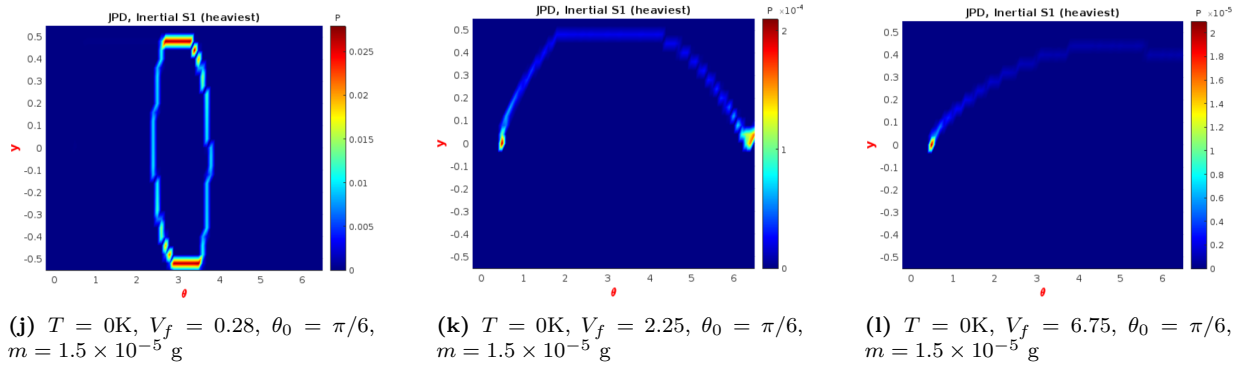
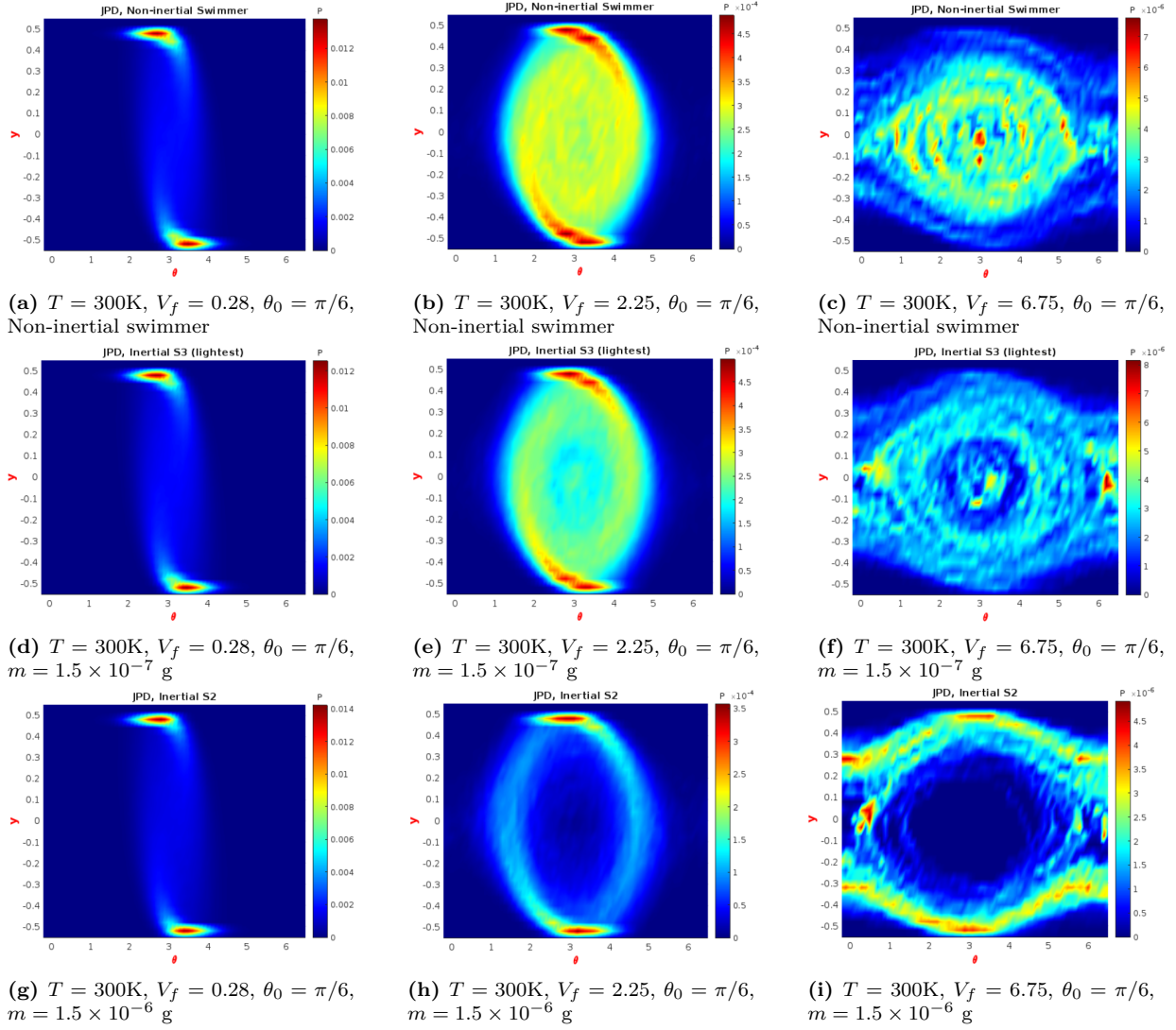


Figure 3.9: Phase portraits displaying the joint probability distribution function (JPDF), $P(\theta, y)$, of four active Brownian particles with varying masses in a microchannel with Poiseuille flow, subjected to varying non-dimensional flow speeds. Inertial S1, Inertial S2, and Inertial S3 refer to the active particles with mass $1.5 \times 10^{-8} \text{ kg}$, $1.5 \times 10^{-9} \text{ kg}$, and $1.5 \times 10^{-10} \text{ kg}$, respectively. The initial condition for all plots is $(X_0, Y_0, \theta_0) = (0, 0, \pi/6)$ and the temperature is 0K.



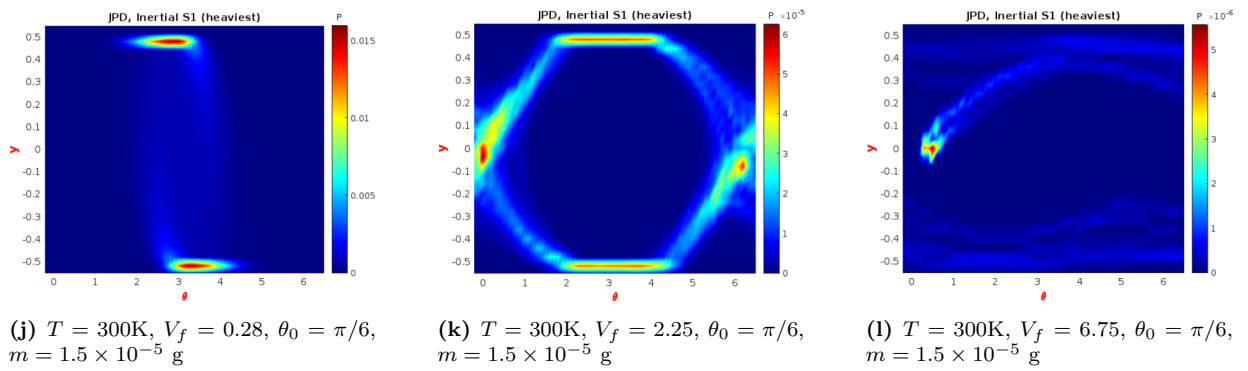
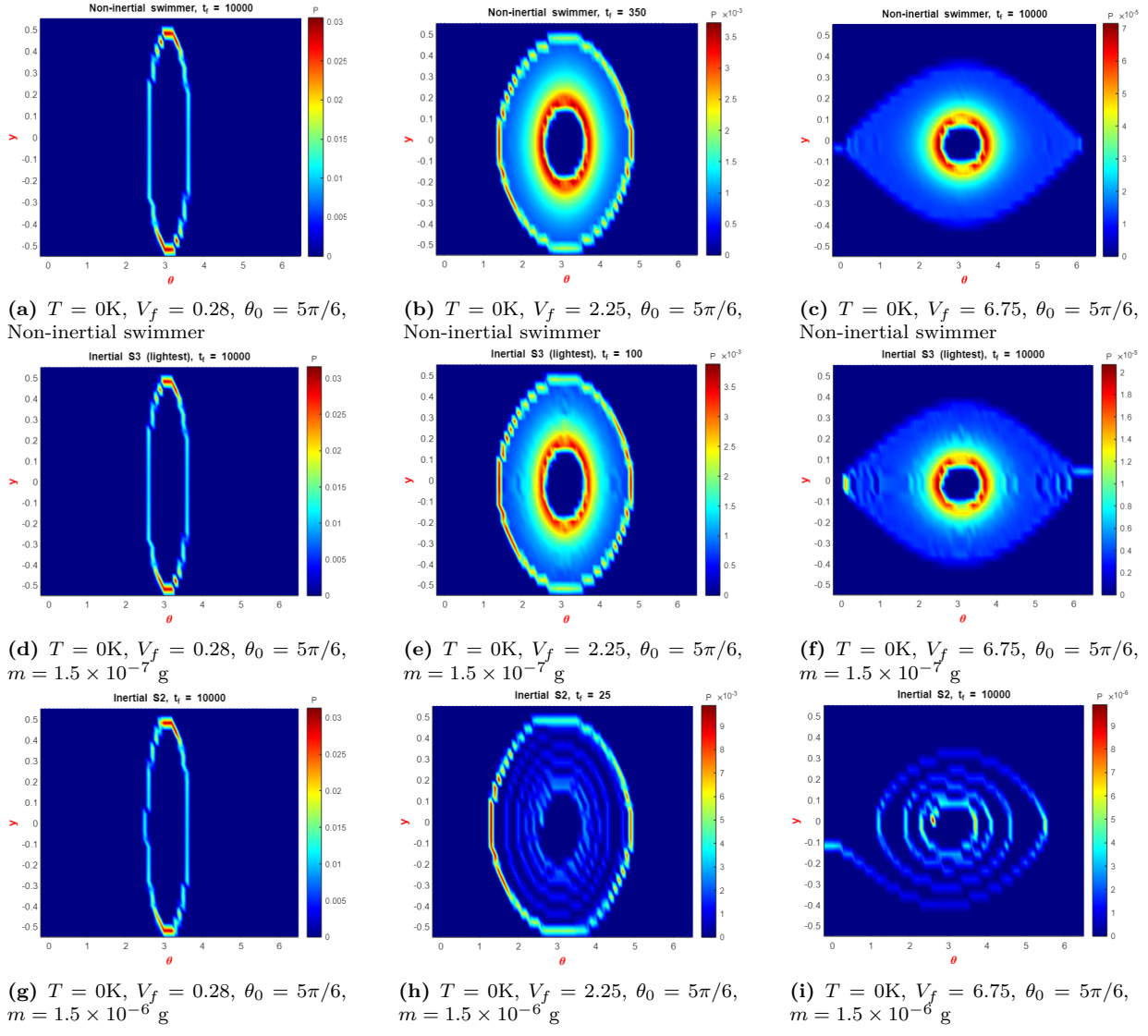


Figure 3.10: Phase portraits displaying the joint probability distribution function (JPDF), $P(\theta, y)$, of four active Brownian particles with varying masses in a microchannel with Poiseuille flow, subjected to varying non-dimensional flow speeds. Inertial S1, Inertial S2, and Inertial S3 refer to the active particles with mass $1.5 \times 10^{-8} \text{ kg}$, $1.5 \times 10^{-9} \text{ kg}$, and $1.5 \times 10^{-10} \text{ kg}$, respectively. The initial condition for all plots is $(X_0, Y_0, \theta_0) = (0, 0, \pi/6)$ and the temperature is 300K.



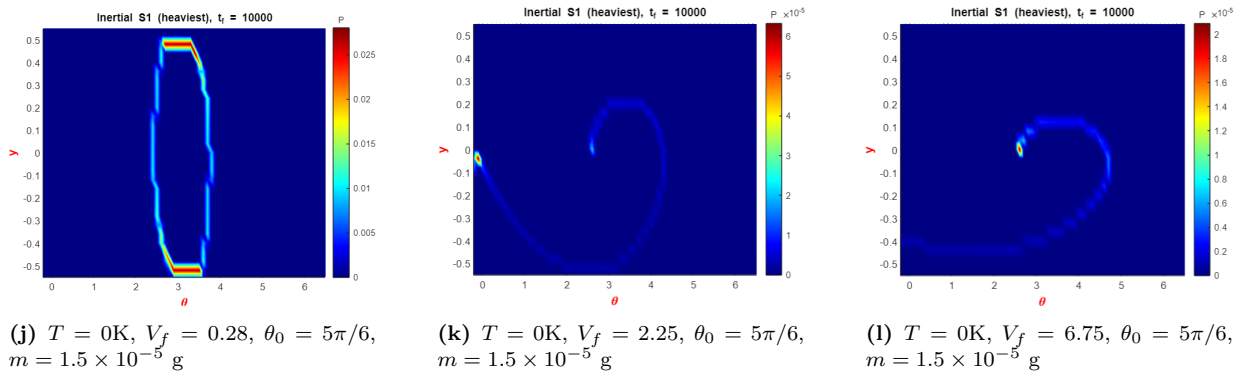
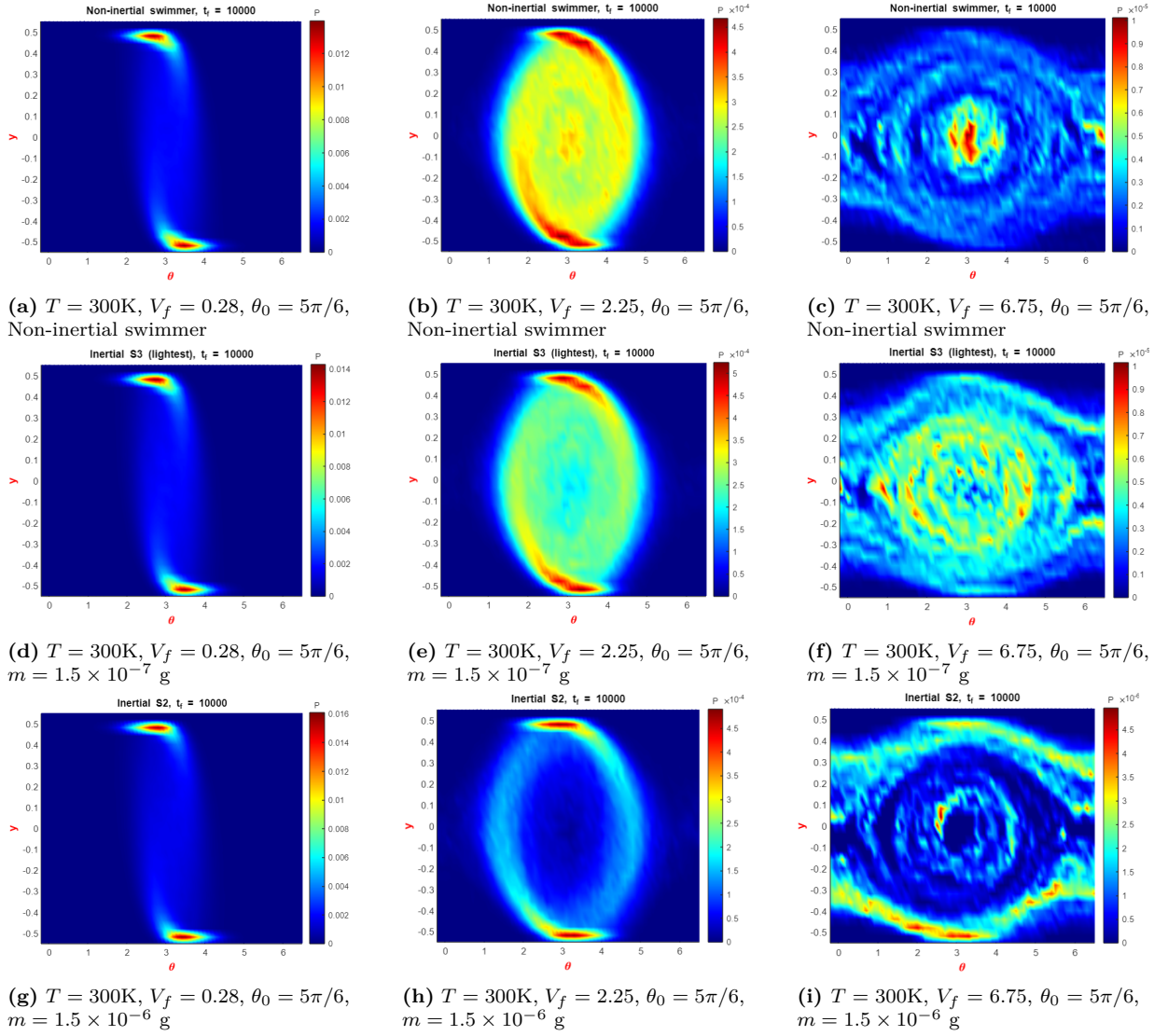


Figure 3.11: Phase portraits displaying the joint probability distribution function (JPDF), $P(\theta, y)$, of four active Brownian particles with varying masses in a microchannel with Poiseuille flow, subjected to varying non-dimensional flow speeds. Inertial S1, Inertial S2, and Inertial S3 refer to the active particles with mass $1.5 \times 10^{-8} \text{ kg}$, $1.5 \times 10^{-9} \text{ kg}$, and $1.5 \times 10^{-10} \text{ kg}$, respectively. The initial condition for all plots is $(X_0, Y_0, \theta_0) = (0, 0, 5\pi/6)$ and the temperature is 0K.



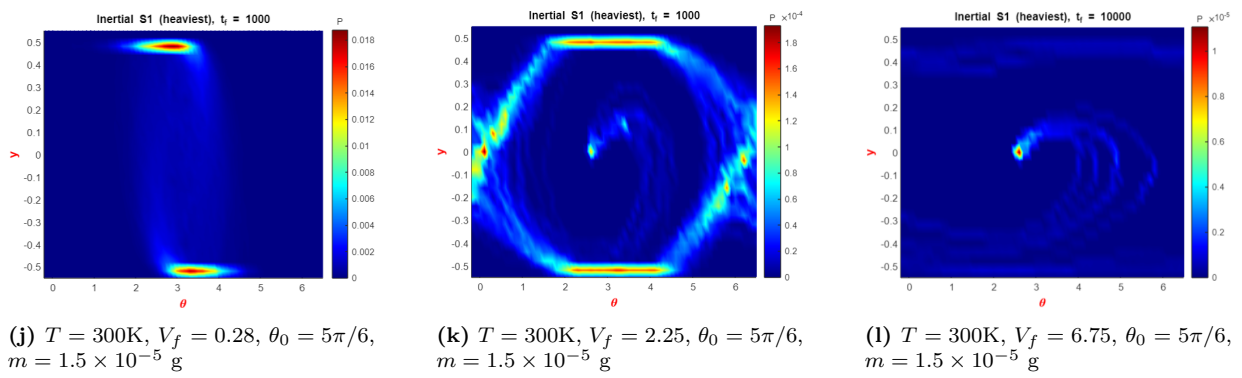


Figure 3.12: Phase portraits displaying the joint probability distribution function (JPDF), $P(\theta, y)$, of four active Brownian particles with varying masses in a microchannel with Poiseuille flow, subjected to varying non-dimensional flow speeds. Inertial S1, Inertial S2, and Inertial S3 refer to the active particles with mass $1.5 \times 10^{-8} \text{ kg}$, $1.5 \times 10^{-9} \text{ kg}$, and $1.5 \times 10^{-10} \text{ kg}$, respectively. The initial condition for all plots is $(X_0, Y_0, \theta_0) = (0, 0, 5\pi/6)$ and the temperature is 300K.

Chapter 4

Appendix

The MATLAB codes and inertial active Brownian particle (ABP) datasets used in this study can be accessed through the repository available at the following link: [Repository for MATLAB Codes and Inertial ABP Datasets](#). Researchers can access the files from this repository to replicate the simulations and perform further analysis on the results presented in this study.

References

- [1] Sriram Ramaswamy. The mechanics and statistics of active matter. *Annu. Rev. Condens. Matter Phys.*, 1(1):323–345, 2010.
- [2] Michael E Cates. Diffusive transport without detailed balance in motile bacteria: does microbiology need statistical physics? *Reports on Progress in Physics*, 75(4):042601, 2012.
- [3] Paweł Romanczuk, Markus Bär, Werner Ebeling, Benjamin Lindner, and Lutz Schimansky-Geier. Active brownian particles: From individual to collective stochastic dynamics. *The European Physical Journal Special Topics*, 202:1–162, 2012.
- [4] Clemens Bechinger, Roberto Di Leonardo, Hartmut Löwen, Charles Reichhardt, Giorgio Volpe, and Giovanni Volpe. Active particles in complex and crowded environments. *Reviews of Modern Physics*, 88(4):045006, 2016.
- [5] Jens Elgeti, Roland G Winkler, and Gerhard Gompper. Physics of microswimmers—single particle motion and collective behavior: a review. *Reports on progress in physics*, 78(5):056601, 2015.
- [6] James P Brody, Paul Yager, Raymond E Goldstein, and Robert H Austin. Biotechnology at low reynolds numbers. *Biophysical journal*, 71(6):3430–3441, 1996.
- [7] Howard C Berg and Douglas A Brown. Chemotaxis in escherichia coli analysed by three-dimensional tracking. *Nature*, 239:500–504, 1972.
- [8] Kyriacos C Leptos, Jeffrey S Guasto, Jerry P Gollub, Adriana I Pesci, and Raymond E Goldstein. Dynamics of enhanced tracer diffusion in suspensions of swimming eukaryotic microorganisms. *Physical Review Letters*, 103(19):198103, 2009.
- [9] Willow R DiLuzio, Linda Turner, Michael Mayer, Piotr Garstecki, Douglas B Weibel, Howard C Berg, and George M Whitesides. Escherichia coli swim on the right-hand side. *Nature*, 435(7046):1271–1274, 2005.

- [10] Ingmar H Riedel, Karsten Kruse, and Jonathon Howard. A self-organized vortex array of hydrodynamically entrained sperm cells. *Science*, 309(5732):300–303, 2005.
- [11] DM Woolley. Motility of spermatozoa at surfaces. *REPRODUCTION-CAMBRIDGE-*, 126(2):259–270, 2003.
- [12] Benjamin M Friedrich and Frank Jülicher. Chemotaxis of sperm cells. *Proceedings of the National Academy of Sciences*, 104(33):13256–13261, 2007.
- [13] Gerhard Gompper, Roland G Winkler, Thomas Speck, Alexandre Solon, Cesare Nardini, Fernando Peruani, Hartmut Löwen, Ramin Golestanian, U Benjamin Kaupp, Luis Alvarez, et al. The 2020 motile active matter roadmap. *Journal of Physics Condensed Matter*, 32(19):193001, 2020.
- [14] Edward M Purcell. Life at low reynolds number. *American journal of physics*, 45(1):3–11, 1977.
- [15] Michael J Lighthill. On the squirming motion of nearly spherical deformable bodies through liquids at very small reynolds numbers. *Communications on pure and applied mathematics*, 5(2):109–118, 1952.
- [16] John R Blake. A spherical envelope approach to ciliary propulsion. *Journal of Fluid Mechanics*, 46(1):199–208, 1971.
- [17] Tapomoy Bhattacharjee and Sujit S Datta. Bacterial hopping and trapping in porous media. *Nature communications*, 10(1):2075, 2019.
- [18] Jeffrey A Riffell and Richard K Zimmer. Sex and flow: the consequences of fluid shear for sperm–egg interactions. *Journal of Experimental Biology*, 210(20):3644–3660, 2007.
- [19] Rachel Levy, David B Hill, M Gregory Forest, and James B Grotberg. Pulmonary fluid flow challenges for experimental and mathematical modeling, 2014.
- [20] AE Patteson, Arvind Gopinath, M Goulian, and PE Arratia. Running and tumbling with e. coli in polymeric solutions. *Scientific reports*, 5(1):15761, 2015.
- [21] Zhenzhong Yang, Dirk AL Aarts, Yi Chen, Shan Jiang, Paula Hammond, Ilona Kretzschmar, Hans-Jorg Schneider, Mohsen Shahinpoor, Axel HE Muller, Chenjie Xu, et al. *Janus particle synthesis, self-assembly and applications*. Royal Society of Chemistry, 2012.

- [22] Andreas Walther and Axel HE Muller. Janus particles: synthesis, self-assembly, physical properties, and applications. *Chemical reviews*, 113(7):5194–5261, 2013.
- [23] Yingjie Wu, Xiankun Lin, Zhiguang Wu, Helmuth Möhwald, and Qiang He. Self-propelled polymer multilayer janus capsules for effective drug delivery and light-triggered release. *ACS applied materials & interfaces*, 6(13):10476–10481, 2014.
- [24] Debabrata Patra, Samudra Sengupta, Wentao Duan, Hua Zhang, Ryan Pavlick, and Ayusman Sen. Intelligent, self-powered, drug delivery systems. *Nanoscale*, 5(4):1273–1283, 2013.
- [25] Mohammad Zarei and Mohanna Zarei. Self-propelled micro/nanomotors for sensing and environmental remediation. *Small*, 14(30):1800912, 2018.
- [26] Jaideep Katuri, Xing Ma, Morgan M Stanton, and Samuel Sánchez. Designing micro- and nanoswimmers for specific applications. *Accounts of chemical research*, 50(1):2–11, 2017.
- [27] Lluís Soler and Samuel Sánchez. Catalytic nanomotors for environmental monitoring and water remediation. *Nanoscale*, 6(13):7175–7182, 2014.
- [28] Larysa Baraban, Denys Makarov, Robert Streubel, Ingolf Monch, Daniel Grimm, Samuel Sanchez, and Oliver G Schmidt. Catalytic janus motors on microfluidic chip: deterministic motion for targeted cargo delivery. *ACS nano*, 6(4):3383–3389, 2012.
- [29] Taro Toyota, Hironori Sugiyama, Soichiro Hiroi, Hiroaki Ito, and Hiroyuki Kitahata. Chemically artificial rovers based on self-propelled droplets in micrometer-scale environment. *Current opinion in colloid & interface science*, 49:60–68, 2020.
- [30] Samuel Sanchez, Alexander A Solovev, Stefan M Harazim, and Oliver G Schmidt. Microbots swimming in the flowing streams of microfluidic channels. *Journal of the American Chemical Society*, 133(4):701–703, 2011.
- [31] Andrea Costanzo, Jens Elgeti, Thorsten Auth, Gerhard Gompper, and Marisol Ripoll. Motility-sorting of self-propelled particles in microchannels. *Europhysics Letters*, 107(3):36003, 2014.
- [32] Bahareh Khezri and Martin Pumera. Metal–organic frameworks based nano/micro/millimeter-sized self-propelled autonomous machines. *Advanced Materials*, 31(14):1806530, 2019.

- [33] Huayu Wu, Dan Zhong, Zhijun Zhang, Yahui Wu, Yunkun Li, Hongli Mao, Kui Luo, Deling Kong, Qiyong Gong, and Zhongwei Gu. A bacteria-inspired morphology genetic biomedical material: self-propelled artificial microbots for metastatic triple negative breast cancer treatment. *ACS nano*, 15(3):4845–4860, 2021.
- [34] Bradley J Nelson and Kathrin E Peyer. Micro-and nanorobots swimming in heterogeneous liquids. *Acs Nano*, 8(9):8718–8724, 2014.
- [35] Huaijuan Zhou, Carmen C Mayorga-Martinez, Salvador Pané, Li Zhang, and Martin Pumera. Magnetically driven micro and nanorobots. *Chemical Reviews*, 121(8):4999–5041, 2021.
- [36] Oncay Yasa, Pelin Erkoc, Yunus Alapan, and Metin Sitti. Microalga-powered microswimmers toward active cargo delivery. *Advanced Materials*, 30(45):1804130, 2018.
- [37] Jing Zheng, Baohu Dai, Jizhuang Wang, Ze Xiong, Ya Yang, Jun Liu, Xiaojun Zhan, Zhihan Wan, and Jinyao Tang. Orthogonal navigation of multiple visible-light-driven artificial microswimmers. *Nature communications*, 8(1):1438, 2017.
- [38] Nikhil Desai, Vaseem A Shaik, and Arezoo M Ardekani. Hydrodynamics-mediated trapping of micro-swimmers near drops. *Soft matter*, 14(2):264–278, 2018.
- [39] Jan Plutnar and Martin Pumera. Chemotactic micro-and nanodevices. *Angewandte Chemie International Edition*, 58(8):2190–2196, 2019.
- [40] Ileana-Alexandra Pavel, Gerardo Salinas, Maciej Mierzwa, Serena Arnaboldi, Patrick Garrigue, and Alexander Kuhn. Cooperative chemotaxis of magnesium microswimmers for corrosion spotting. *ChemPhysChem*, 22(13):1321–1325, 2021.
- [41] Melville S Green. Brownian motion in a gas of noninteracting molecules. *The Journal of Chemical Physics*, 19(8):1036–1046, 1951.
- [42] Pinaki Chatterjee, Lars Hernquist, and Abraham Loeb. Brownian motion in gravitationally interacting systems. *Physical review letters*, 88(12):121103, 2002.
- [43] TJ Murphy and JL Aguirre. Brownian motion of n interacting particles. i. extension of the einstein diffusion relation to the n-particle case. *The Journal of Chemical Physics*, 57(5):2098–2104, 1972.
- [44] PN Segre, OP Behrend, and PN Pusey. Short-time brownian motion in colloidal suspensions: Experiment and simulation. *Physical Review E*, 52(5):5070, 1995.

- [45] Gerhard A Schumacher and Theodorus GM van de Ven. Brownian motion of charged colloidal particles surrounded by electric double layers. *Faraday Discussions of the Chemical Society*, 83:75–85, 1987.
- [46] Bernard H Lavenda. Brownian motion. *Scientific American*, 252(2):70–85, 1985.
- [47] Daniel Lavalette, Mark A Hink, Martine Tourbez, Catherine Tetreau, and Antonie J Visser. Proteins as micro viscosimeters: Brownian motion revisited. *European Biophysics Journal*, 35:517–522, 2006.
- [48] Adam E Cohen and WE Moerner. Controlling brownian motion of single protein molecules and single fluorophores in aqueous buffer. *Optics express*, 16(10):6941–6956, 2008.
- [49] Dmytro Nykypanchuk, Helmut H Strey, and David A Hoagland. Brownian motion of dna confined within a two-dimensional array. *Science*, 297(5583):987–990, 2002.
- [50] Maged F Serag and Satoshi Habuchi. Conserved linear dynamics of single-molecule brownian motion. *Nature Communications*, 8(1):15675, 2017.
- [51] M Reza Shaebani, Adam Wysocki, Roland G Winkler, Gerhard Gompper, and Heiko Rieger. Computational models for active matter. *Nature Reviews Physics*, 2(4):181–199, 2020.
- [52] L Hecht, JC Ureña, and B Liebchen. An introduction to modeling approaches of active matter. *arXiv preprint arXiv:2102.13007*, 2021.
- [53] Borge ten Hagen, Sven van Teeffelen, and Hartmut Löwen. Brownian motion of a self-propelled particle. *Journal of Physics: Condensed Matter*, 23(19):194119, 2011.
- [54] Francisco J Sevilla and Mario Sandoval. Smoluchowski diffusion equation for active brownian swimmers. *Physical Review E*, 91(5):052150, 2015.
- [55] Alexandre P Solon, Joakim Stenhammar, Raphael Wittkowski, Mehran Kardar, Yariv Kafri, Michael E Cates, and Julien Tailleur. Pressure and phase equilibria in interacting active brownian spheres. *Physical review letters*, 114(19):198301, 2015.
- [56] Isabella Petrelli, Pasquale Digregorio, Leticia F Cugliandolo, Giuseppe Gonnella, and Antonio Suma. Active dumbbells: Dynamics and morphology in the coexisting region. *The European Physical Journal E*, 41:1–23, 2018.

- [57] Lorenzo Caprini, Umberto Marini Bettolo Marconi, Claudio Maggi, Matteo Paoluzzi, and Andrea Puglisi. Hidden velocity ordering in dense suspensions of self-propelled disks. *Physical Review Research*, 2(2):023321, 2020.
- [58] Xia-qing Shi, Giordano Fausti, Hugues Chaté, Cesare Nardini, and Alexandre Solon. Self-organized critical coexistence phase in repulsive active particles. *Physical Review Letters*, 125(16):168001, 2020.
- [59] Juan Ruben Gomez-Solano and Francisco J Sevilla. Active particles with fractional rotational brownian motion. *Journal of Statistical Mechanics: Theory and Experiment*, 2020(6):063213, 2020.
- [60] José Martin-Roca, Raul Martinez, Lachlan C Alexander, Angel Luis Diez, Dirk GAL Aarts, Francisco Alarcon, Jorge Ramírez, and Chantal Valeriani. Characterization of mips in a suspension of repulsive active brownian particles through dynamical features. *The Journal of Chemical Physics*, 154(16):164901, 2021.
- [61] Alexander R Sprenger, Christian Bair, and Hartmut Löwen. Active brownian motion with memory delay induced by a viscoelastic medium. *Physical Review E*, 105(4):044610, 2022.
- [62] Ivo Buttinoni, Julian Bialké, Felix Kümmel, Hartmut Löwen, Clemens Bechinger, and Thomas Speck. Dynamical clustering and phase separation in suspensions of self-propelled colloidal particles. *Physical review letters*, 110(23):238301, 2013.
- [63] Jeremie Palacci, Stefano Sacanna, Asher Preska Steinberg, David J Pine, and Paul M Chaikin. Living crystals of light-activated colloidal surfers. *Science*, 339(6122):936–940, 2013.
- [64] Igor S Aranson. Active colloids. *Physics-Uspekhi*, 56(1):79, 2013.
- [65] Sho C Takatori, Raf De Dier, Jan Vermant, and John F Brady. Acoustic trapping of active matter. *Nature communications*, 7(1):10694, 2016.
- [66] Andreas Zöttl and Holger Stark. Emergent behavior in active colloids. *Journal of Physics: Condensed Matter*, 28(25):253001, 2016.
- [67] Peter Friedl and Darren Gilmour. Collective cell migration in morphogenesis, regeneration and cancer. *Nature reviews Molecular cell biology*, 10(7):445–457, 2009.

- [68] Volker Bormuth, Vladimir Varga, Jonathon Howard, and Erik Schäffer. Protein friction limits diffusive and directed movements of kinesin motors on microtubules. *science*, 325(5942):870–873, 2009.
- [69] Volker Schaller, Christoph Weber, Christine Semmrich, Erwin Frey, and Andreas R Bausch. Polar patterns of driven filaments. *Nature*, 467(7311):73–77, 2010.
- [70] Tamás Vicsek and Anna Zafeiris. Collective motion. *Physics reports*, 517(3-4):71–140, 2012.
- [71] Hartmut Löwen. Inertial effects of self-propelled particles: From active brownian to active langevin motion. *The Journal of chemical physics*, 152(4):040901, 2020.
- [72] Marc Joyeux and Eric Bertin. Pressure of a gas of underdamped active dumbbells. *Physical Review E*, 93(3):032605, 2016.
- [73] Bao-Quan Ai and Feng-Guo Li. Transport of underdamped active particles in ratchet potentials. *Soft matter*, 13(13):2536–2542, 2017.
- [74] Suraj Shankar and M Cristina Marchetti. Hidden entropy production and work fluctuations in an ideal active gas. *Physical Review E*, 98(2):020604, 2018.
- [75] Suvendu Mandal, Benno Liebchen, and Hartmut Löwen. Motility-induced temperature difference in coexisting phases. *Physical review letters*, 123(22):228001, 2019.
- [76] Caleb G Wagner, Michael F Hagan, and Aparna Baskaran. Response of active brownian particles to boundary driving. *Physical Review E*, 100(4):042610, 2019.
- [77] Hidde Derk Vuijk, Jens-Uwe Sommer, Holger Merlitz, Joseph Michael Brader, and Abhinav Sharma. Lorentz forces induce inhomogeneity and flux in active systems. *Physical Review Research*, 2(1):013320, 2020.
- [78] Viktor Holubec and Rahul Marathe. Underdamped active brownian heat engine. *Physical Review E*, 102(6):060101, 2020.
- [79] Jonas Mayer Martins and Raphael Wittkowski. Inertial dynamics of an active brownian particle. *Physical Review E*, 106(3):034616, 2022.
- [80] Christian Scholz, Soudeh Jahanshahi, Anton Ldov, and Hartmut Löwen. Inertial delay of self-propelled particles. *Nature communications*, 9(1):1–9, 2018.

- [81] Emanuele Crosato, Mikhail Prokopenko, and Richard E Spinney. Irreversibility and emergent structure in active matter. *Physical Review E*, 100(4):042613, 2019.
- [82] Luis L Gutierrez-Martinez and Mario Sandoval. Inertial effects on trapped active matter. *The Journal of Chemical Physics*, 153(4):044906, 2020.
- [83] Pedro Herrera and Mario Sandoval. Maxwell-boltzmann velocity distribution for noninteracting active matter. *Physical Review E*, 103(1):012601, 2021.
- [84] Alexander R Sprenger, Soudeh Jahanshahi, Alexei V Ivlev, and Hartmut Löwen. Time-dependent inertia of self-propelled particles: The langevin rocket. *Physical Review E*, 103(4):042601, 2021.
- [85] Lukas Hecht, Suvendu Mandal, Hartmut Löwen, and Benno Liebchen. Active refrigerators powered by inertia. *Physical Review Letters*, 129(17):178001, 2022.
- [86] EA Lisin, OS Vaulina, II Lisina, and OF Petrov. Motion of a self-propelled particle with rotational inertia. *Physical Chemistry Chemical Physics*, 24(23):14150–14158, 2022.
- [87] Alexander R Sprenger, Lorenzo Caprini, Hartmut Löwen, and René Wittmann. Dynamics of active particles with translational and rotational inertia. *arXiv preprint arXiv:2301.01865*, 2023.
- [88] Olivier Dauchot and Vincent Démery. Dynamics of a self-propelled particle in a harmonic trap. *Physical review letters*, 122(6):068002, 2019.
- [89] A. Deblais, T. Barois, T. Guerin, P. H. Delville, R. Vaudaine, J. S. Lintu-vuori, J. F. Boudet, J. C. Baret, and H. Kellay. Boundaries control collective dynamics of inertial self-propelled robots. *Phys. Rev. Lett.*, 120:188002, May 2018. doi: 10.1103/PhysRevLett.120.188002. URL <https://link.aps.org/doi/10.1103/PhysRevLett.120.188002>.
- [90] Mickael Bourgoin, Ronan Kervil, Cecile Cottin-Bizonne, Florence Raynal, Romain Volk, and Christophe Ybert. Kolmogorovian active turbulence of a sparse assembly of interacting marangoni surfers. *Physical Review X*, 10(2):021065, 2020.
- [91] Marco Leoni, Matteo Paoluzzi, Sarah Eldeen, Anthony Estrada, Lauren Nguyen, Maria Alexandrescu, Karin Sherb, and Wylie W Ahmed. Surfing and crawling macroscopic active particles under strong confinement: Inertial dynamics. *Physical Review Research*, 2(4):043299, 2020.

- [92] Lorenzo Caprini and Umberto Marini Bettolo Marconi. Inertial self-propelled particles. *The Journal of Chemical Physics*, 154(2):024902, 2021.
- [93] M Muhsin and M Sahoo. Inertial active ornstein-uhlenbeck particle in the presence of a magnetic field. *Physical Review E*, 106(1):014605, 2022.
- [94] N Arsha, KP Jepsin, and M Sahoo. Steady state correlations and induced trapping of an inertial aoup particle. *arXiv preprint arXiv:2208.14443*, 2022.
- [95] Wen-Zhen Fang, Seokgyun Ham, Rui Qiao, and Wen-Quan Tao. Magnetic actuation of surface walkers: The effects of confinement and inertia. *Langmuir*, 36(25):7046–7055, 2020.
- [96] Narender Khatri and Raymond Kapral. Inertial effects on rectification and diffusion of active brownian particles in an asymmetric channel. *arXiv preprint arXiv:2301.02902*, 2023.
- [97] Narender Khatri and PS Burada. Diffusion of chiral active particles in a poiseuille flow. *Physical Review E*, 105(2):024604, 2022.
- [98] Andreas Zöttl and Holger Stark. Nonlinear dynamics of a microswimmer in poiseuille flow. *Physical review letters*, 108(21):218104, 2012.
- [99] Giorgio Volpe, Sylvain Gigan, and Giovanni Volpe. Simulation of the active brownian motion of a microswimmer. *American Journal of Physics*, 82(7):659–664, 2014.
- [100] Pulak K Ghosh, Vyacheslav R Misko, Fabio Marchesoni, and Franco Nori. Self-propelled janus particles in a ratchet: Numerical simulations. *Physical review letters*, 110(26):268301, 2013.
- [101] CJ Olson Reichhardt and Charles Reichhardt. Ratchet effects in active matter systems. *Annual Review of Condensed Matter Physics*, 8:51–75, 2017.
- [102] Giorgio Volpe and Giovanni Volpe. Simulation of a brownian particle in an optical trap. *American Journal of Physics*, 81(3):224–230, 2013.
- [103] Agnese Callegari and Giovanni Volpe. Numerical simulations of active brownian particles. *Flowing Matter*, page 211, 2019.
- [104] Kai Qi, Hemalatha Annepu, Gerhard Gompper, and Roland G Winkler. Rheotaxis of spheroidal squirmers in microchannel flow: Interplay of shape, hydrodynamics, active stress, and thermal fluctuations. *Physical Review Research*, 2(3):033275, 2020.

- [105] Andreas Zöttl. Hydrodynamics of microswimmers in confinement and in poiseuille flow. 2014.
- [106] Akash Choudhary, Subhechchha Paul, Felix Rühle, and Holger Stark. How inertial lift affects the dynamics of a microswimmer in poiseuille flow. *Communications Physics*, 5(1):1–9, 2022.
- [107] Shiyan Wang and AM Ardekani. Unsteady swimming of small organisms. *Journal of Fluid Mechanics*, 702:286–297, 2012.
- [108] Amandine Hamel, Cathy Fisch, Laurent Combettes, Pascale Dupuis-Williams, and Charles N Baroud. Transitions between three swimming gaits in paramecium escape. *Proceedings of the National Academy of Sciences*, 108(18):7290–7295, 2011.
- [109] S Wang and A Ardekani. Inertial squirmer. *Physics of Fluids*, 24(10):101902, 2012.
- [110] Aditya S Khair and Nicholas G Chisholm. Expansions at small reynolds numbers for the locomotion of a spherical squirmer. *Physics of Fluids*, 26(1):011902, 2014.
- [111] Liqiang Ren, Nitesh Nama, Jeffrey M McNeill, Fernando Soto, Zhifei Yan, Wu Liu, Wei Wang, Joseph Wang, and Thomas E Mallouk. 3d steerable, acoustically powered microswimmers for single-particle manipulation. *Science advances*, 5(10):eaax3084, 2019.
- [112] Amirreza Aghakhani, Oncay Yasa, Paul Wrede, and Metin Sitti. Acoustically powered surface-slipping mobile microrobots. *Proceedings of the National Academy of Sciences*, 117(7):3469–3477, 2020.
- [113] Christina Kurzthaler and Howard A Stone. Microswimmers near corrugated, periodic surfaces. *Soft matter*, 17(12):3322–3332, 2021.
- [114] Saverio E Spagnolie and Eric Lauga. Hydrodynamics of self-propulsion near a boundary: predictions and accuracy of far-field approximations. *Journal of Fluid Mechanics*, 700:105–147, 2012.
- [115] Jonathan R Howse, Richard AL Jones, Anthony J Ryan, Tim Gough, Reza Vafabakhsh, and Ramin Golestanian. Self-motile colloidal particles: from directed propulsion to random walk. *Physical review letters*, 99(4):048102, 2007.
- [116] EA Lisin, OS Vaulina, II Lisina, and OF Petrov. Active brownian particle in homogeneous media of different viscosities: Numerical simulations. *Physical Chemistry Chemical Physics*, 23(30):16248–16257, 2021.

- [117] Giuseppe Negro, C Basilio Caporusso, Pasquale Digregorio, Giuseppe Gonnella, Antonio Lamura, and Antonio Suma. Hydrodynamic effects on the liquid-hexatic transition of active colloids. *The European Physical Journal E*, 45(9):75, 2022.
- [118] Soumen De Karmakar, Anshika Chugh, and Rajaraman Ganesh. Collective behavior of soft self-propelled disks with rotational inertia. *Scientific Reports*, 12(1):22563, 2022.
- [119] J Majdalani. Exact navier-stokes solution for the pulsatory viscous channel flow with arbitrary pressure gradient. *Journal of propulsion and power*, 24(6):1412–1423, 2008.
- [120] Steffen M Recktenwald, Christian Wagner, and Thomas John. Optimizing pressure-driven pulsatile flows in microfluidic devices. *Lab on a Chip*, 21(13):2605–2613, 2021.
- [121] Ronald L Panton. *Incompressible flow*. John Wiley & Sons, 2013.
- [122] Alexander Hope, Ottavio A Croze, Wilson CK Poon, Martin A Bees, and Mark D Haw. Resonant alignment of microswimmer trajectories in oscillatory shear flows. *Physical Review Fluids*, 1(5):051201, 2016.
- [123] Crispin W Gardiner et al. *Handbook of stochastic methods*, volume 3. springer Berlin, 1985.